

2017

# Numerical Solutions of the Radiosity Equation by the Galerkin Method for the Spherical Pyramid (Mars Project)

Qiuyang Deng

Roger Williams University, [qdeng163@g.rwu.edu](mailto:qdeng163@g.rwu.edu)

Follow this and additional works at: [http://docs.rwu.edu/math\\_theses](http://docs.rwu.edu/math_theses)



Part of the [Applied Mathematics Commons](#)

---

## Recommended Citation

Deng, Qiuyang, "Numerical Solutions of the Radiosity Equation by the Galerkin Method for the Spherical Pyramid (Mars Project)" (2017). *Mathematics Theses*. 4.

[http://docs.rwu.edu/math\\_theses/4](http://docs.rwu.edu/math_theses/4)

This Thesis is brought to you for free and open access by the Feinstein College of Arts and Sciences Theses at DOCS@RWU. It has been accepted for inclusion in Mathematics Theses by an authorized administrator of DOCS@RWU. For more information, please contact [mwu@rwu.edu](mailto:mwu@rwu.edu).

*Numerical Solutions of the Radiosity Equation by the Galerkin Method  
for the Spherical Pyramid (Mars Project)*

*September, 2015- April, 2017*

*Deng, Qiuyang*

*Advisor: Dr. Yajni Warnapala*

*Applied Mathematics (Bachelor of Science)*

*Mathematics Department*

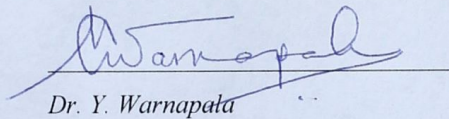
Feinstein College of Arts and Sciences

Roger Williams University

*May 2017*

The thesis of *(Qiuyang Deng)* was reviewed and approved by the following:

---

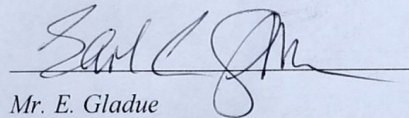


*Dr. Y. Warnapata*

*Chair, Professor of Mathematics*

*Thesis advisor*

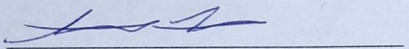
Date 17<sup>th</sup> of April '17



*Mr. E. Gladue*

*Professor of Mathematics*

Date 13 April 2017



*Dr. S. Rutherford*

*Professor of Environmental Science*

Date 4/13/17

## **Acknowledgements**

I would like to thank Dr. Warnapala for her mentorship, appreciate Prof. Gladue and Prof. Rutherford for their feedback and suggestions, appreciate Ms. Kennedy for her technical support, and also greatly appreciate the financial support from the Provost's Fund of Roger Williams University.

# Table of Contents

Acknowledgements.....	iii
Abstract.....	ix
<b>1 Introduction.....</b>	<b>1</b>
<b>1.1 Radiosity Model (Brightness Equation).....</b>	<b>2</b>
<b>1.2 Kernel- Function .....</b>	<b>3</b>
<b>2 Galerkin Method .....</b>	<b>5</b>
<b>2.1 Finite-Element Method .....</b>	<b>5</b>
<b>2.2 Method of Mean Weighted Residuals .....</b>	<b>6</b>
<b>2.3 Galerkin Method of Weighted Residuals .....</b>	<b>6</b>
<b>2.4 Gaussian Quadrature .....</b>	<b>8</b>
<b>2.5 Basis Function.....</b>	<b>10</b>
<b>3 The Spherical Shapes .....</b>	<b>12</b>
<b>4 Numerical Results (Part I).....</b>	<b>14</b>
<b>4.1 The Errors for Different Degrees and Nodes .....</b>	<b>14</b>
<b>4.2 The Errors of the Two Spherical Shapes .....</b>	<b>16</b>
<b>5 The Lighting and Brightness for Radiosity .....</b>	<b>19</b>
<b>5.1 Mars Background.....</b>	<b>19</b>
<b>5.2 Measuring Light Levels.....</b>	<b>20</b>
<b>6 Realistic Applications.....</b>	<b>24</b>
<b>6.1 The Errors of the Two Spherical Shapes for Practical Reflectivity Values.....</b>	<b>24</b>
<b>6.2 Final Shape: Spherical Pyramid.....</b>	<b>24</b>
<b>6.3 Consideration of Coordinate Point on Mars .....</b>	<b>25</b>
<b>6.4 The Errors under Larger Reflectivity Values .....</b>	<b>28</b>
<b>6.5 Consideration of Emissivity Functions (True Functions).....</b>	<b>29</b>
<b>6.6 The Revised Spherical Pyramid .....</b>	<b>32</b>
<b>6.7 The Numerical Results (Part III).....</b>	<b>33</b>
<b>7 Future Directions/Work.....</b>	<b>35</b>
<b>8 References .....</b>	<b>37</b>
<b>9 Appendices .....</b>	<b>38</b>
<b>9.1 Fredholm Integral Equation of the Second Kind.....</b>	<b>38</b>

9.2	<b><i>Galerkin Method</i></b> .....	39
9.3	<b><i>The Adomian Decomposition Method</i></b> .....	41
9.4	<b><i>The Modified Decomposition Method</i></b> .....	44
9.5	<b><i>The Volume and Surface Area of the Spherical Pyramid</i></b> .....	46
9.6	<b><i>The Weakly-Singular Fredholm Integral Equations</i></b> .....	49
9.7	<b><i>The Weakly-Singular Fredholm Integral Equations (Nonlinear)</i></b> .....	51

**Table 4.1** Using the Galerkin Method, convergence errors were calculated for five random points. Interior nodes were defaulted to 16, and exterior nodes were defaulted to 8. The value of the degree of the boundary function varied from 3 to 7. .... 14

**Table 4.2** Using the Galerkin Method, convergence errors were calculated for five random points. The degree was set to be 5, and exterior nodes were defaulted to 8. The values of interior nodes varied from 16 to 32. .... 15

**Table 4.3** Using the Galerkin Method, convergence errors were calculated for five random points. The degree was set to be 5, and the interior nodes were set to be 16. The values of exterior nodes varied from 8 to 20..... 15

**Table 4.4** Using the Galerkin Method, convergence errors were calculated for five random points with different reflectivity values ranging from  $5 \times 10^{-5}$  to  $4 \times 10^{-7}$  for the Spherical Cone. 16

**Table 4.5** Using the Galerkin Method, convergence errors were calculated for five random points with different reflectivity values ranging from  $8.00 \times 10^{-2}$  to  $1.00 \times 10^{-10}$  for the Spherical Rhombus..... 17

**Table 5.1** Common illumination levels available from the Engineering Toolbox..... 21

**Table 5.2** Recommended light levels for different activities from the illuminating Engineering Society..... 22

<b>Table 6.1</b> the convergence errors of two spherical shapes when the reflectivity values were set to be 0.005.....	24
<b>Table 6.2</b> The distance of different atmospheric layers from Earth and Mars.....	26
<b>Table 6.3</b> The coordinate points corresponding to the Earth atmospheric layers, the unit of distance is km.....	27
<b>Table 6.4</b> Using the Galerkin Method (degree of 5), convergence errors were calculated for four random distances with different reflectivity values (0.001 and 0.0005) and three emissivity functions (also called True Function) for the Spherical Pyramid. ....	28
<b>Table 6.5</b> Using the Galerkin Method (degree of 5), convergence errors were calculated for four random distances with reflectivity values at 0.005 and five emissivity functions (also called True Function) for the Spherical Pyramid. ....	32
<b>Table 6.6</b> Using the Galerkin Method (degree of 7), convergence errors were calculated for four random distances with reflectivity values at 0.01 and five true functions for the Spherical Pyramid.....	33
<b>Table 7.1</b> Relative solar intensity of different planets comparing with the intensity of Earth, due to different distances from the sun only. ....	35
<b>Figure 3.1</b> Spherical Cone, the first designed shape for studying Radiosity Equation.....	12
<b>Figure 3.2</b> Spherical Rhombus, the second designed shape for studying Radiosity Equation ....	12
<b>Figure 4.1</b> Convergence errors of the Spherical Cone and Spherical Rhombus. The range of reflectivity values varied from $5 \times 10^{-5}$ to $4 \times 10^{-7}$ .....	18
<b>Figure 5.1</b> Constitutions of the “brightness” of light .....	20
<b>Figure 6.1</b> Spherical Pyramid, the third designed shape for studying the Radiosity Model .....	25

<b>Figure 6.2</b> Atmospheric layers on Mars.....	27
<b>Figure 6.3</b> Convergence errors of the Spherical Pyramid with different emissivity functions. Shades of purple represent errors for the reflectivity value of 0.001, and shades of green represent errors for the reflectivity value of 0.0005.....	29
<b>Figure 6.4</b> $\varepsilon = \sin(\pi x)$ .....	30
<b>Figure 6.5</b> $\varepsilon = 0.0001\cos^2(0.01x)$ .....	30
<b>Figure 6.6</b> $\varepsilon = 0.0001\cos^2(0.01x) + 0.0001\sin^2(0.01x)$ .....	31
<b>Figure 6.7</b> $\varepsilon = 0.0001\sin(x) + 0.0001\cos(x)$ .....	31
<b>Figure 6.8</b> The change of the Spherical Pyramid caused by the change of coefficients.....	32
<b>Figure 6.9</b> Convergence errors of the Spherical Pyramid with different emissivity functions. The errors of $\sin(\pi x)$ and $0.0001\sin(x) + 0.0001\cos(x)$ were too close to each other. Therefore, it was difficult to visualize the difference on the graph. ....	34
<b>Equation 1.1</b> Mathematical Model: the Radiosity Equation.....	2
<b>Equation 1.2</b> Fredholm Integral Equation of the Second Kind.....	3
<b>Equation 1.3</b> The Kernel term: G-function .....	3
<b>Equation 2.1</b> The form of inner product of Galerkin Method of Weighted Residuals .....	6
<b>Equation 2.2</b> The set of all basis functions of the Galerkin Method of Weighted Residuals .....	7
<b>Equation 2.3</b> The form of the linear combination of basis functions .....	7
<b>Equation 2.4</b> The form of the Lagrange interpolating polynomial .....	9
<b>Equation 2.5</b> The Quadrature formula.....	9
<b>Equation 2.6</b> The form of the Trapezoidal Rule.....	9
<b>Equation 2.7</b> The form of the Simpson's Rule.....	9



*Equation 2.8* Change of interval by applying the Gaussian quadrature ..... 10

*Equation 2.9* Basis functions: the spherical harmonic functions..... 11

*Equation 2.10* The form of the general solution for the Radiosity Equation by the Galerkin  
Method ..... 11

*Equation 6.1* The basic form of the sine wave function ..... 30

# Abstract

The Radiosity of a surface is the rate at which energy leaves that surface. It includes the energy emitted by a surface as well as the energy reflected. In this thesis, a spherical shaped interior space was designed on a spacecraft, which one day might land on Mars. The Radiosity model was used to determine the brightness inside the space. A global Galerkin method is used to solve the Radiosity Equation for several spherical shapes. This research is based on the study of the Radiosity Equation for occluded surfaces using the Collocation Method by Atkinson and Chein. The previous research was done on the Sphere, Perturbation of the Sphere, Ellipsoid and the Oval of Cassini. The convergence errors between true solutions and approximated numerical solutions for different reflectivity values and emissivity functions were presented.

# 1 Introduction

The purpose of this project is to design a spherical interior space (room) on a spacecraft that one day might land on Mars. The reason for constructing this type of a room is to achieve the maximum light efficiency. The “Radiosity Equation (/Model)” was used to determine how much brightness (light energy) will be emitted and reflected from the designed spherical room. In this research, we considered the brightness from the Martian atmosphere where emissivity and reflectivity are inversely proportional.

Atkinson and Chein studied the Radiosity equation for occluded surfaces using the collocation method based on piecewise polynomial interpolation. Theoretical results were examined including questions of super-convergence of the collocation solution. The use of “discontinuity meshing” was examined for both piecewise constant and piecewise linear collocation.<sup>1</sup> In 2000, Atkinson studied the planar Radiosity equation by using a matrix-vector multiplication method. The numerical results presented the regularity properties of the Radiosity solution, including both the effects of the corners and the visibility function.<sup>2</sup> Voigt et al. solved the Radiosity equation by an adaptive finite element method and linked it to heat conduction. The numerical method used in computer graphics to solve global illumination problems was applied to heat radiation.<sup>3</sup> Much of the work done in integral equations in the past used a finite element framework in solving the integral equation. The resulting numerical methods were quite flexible for a large variety of surfaces, but often they converge slowly.

In this paper, we determined the brightness of a room on the spacecraft, and we considered the sunlight to be the only light source for our research. The Galerkin Method of Weighted Residuals

---

<sup>1</sup> Ref [12]

<sup>2</sup> Ref [13]

<sup>3</sup> Ref [15]

was used to solve the Radiosity Equation. The convergence errors between the true solutions and approximated solutions for different spherical shapes are presented.

### ***1.1 Radiosity Equation (Brightness Equation)***

The Radiosity equation generally describes the energy both emitted from and reflected by a surface. The amount of energy which can be emitted from a surface, depends only on the temperature of the surface (the Stefan-Boltzmann Law and the Wien’s Law) and the emissivity of the material. The energy which strikes the surface, is reflected from the surrounding environment. The illumination at a given point in the environment is a combination of the light emitted by a light source, and the light reflected from the surfaces.

The Radiosity Model (shown below) is a mathematical model for the brightness of a collection of one or more surfaces, with given reflectivity and emissivity.

$$u(P) - \frac{\rho(P)}{\pi} \int_S u(Q)G(P, Q)V(P, Q)dS_Q = E(P), P \in S$$

***Equation 1.1 Mathematical Model: the Radiosity Equation***

To be more specific,  $P$  is an interior point on the boundary of the surface, and  $Q$  is an exterior point.  $u(P)$  is the brightness at  $P$ , while  $E(P)$  is the emissivity, the measure of an object’s ability to emit energy.  $\rho(P)$  is the reflectivity (from 0 to 1), the fraction of incident energy reflected by the surfaces made of different materials.  $S$  is a closed bounded surface in three dimensions and assumed to be a Lambertian diffuse reflector. According to Lambert’s Law, if a surface is defined to be a “diffuse reflector”, any light energy which strikes the surface will be reflected in all directions, dependent only on the angle between the surfaces’ normal and the incoming light vector. Under the assumption of constant brightness, the  $V(P, Q)$  is an unclouded surface and assumed to be 1. The term  $G(P, Q)$  is the Kernel term, which would be explained below.

## 1.2 Kernel- Function

The partial integral in the Radiosity model is a Fredholm integral equation of the Second Kind.

In mathematics, the Fredholm integral equation is an integral equation with a Kernel K, a compact operator where the solution gives rise to the Fredholm theory<sup>4</sup>.

$$\phi(t) = f(t) + \lambda \int_a^b K(t,s)\phi(s)ds$$

*Equation 1.2 Fredholm Integral Equation of the Second Kind*

The general form of a Fredholm integral equation of the Second Kind is shown in **Equation 1.2**, which the partial integral of the Radiosity model is matched with the form of the Fredholm equation. In the Radiosity model,  $u(P)$  is the term “ $\phi(t)$ ” that we intend to solve.  $E(P)$ , the emissivity function in the Radiosity model, is the  $f(t)$ . The reflectivity  $\frac{\rho(P)}{\pi}$  is the  $\lambda$ .

To solve  $u(P)$ , we need to integrate  $u(Q)$  with respect to  $Q$  in a closed bounded surface at an exterior point. The Kernel K is defined as  $G(P, Q)$  in the Radiosity Equation.  $G(P, Q)$  is given by:

$$G(P, Q) = \frac{\cos(\theta_P) \cdot \cos(\theta_Q)}{|P - Q|^2} = \frac{[(Q - P) \cdot n_P][(P - Q) \cdot n_Q]}{|P - Q|^4}$$

*Equation 1.3 The Kernel term: G-function*

where  $n_P$  and  $n_Q$  are the inner unit normals to S at P and Q respectively. In this case, the Kernel term is weakly-singular<sup>5</sup> and proved by the following:

let  $P = (p_1, p_2, p_3)$ , and  $Q = (q_1, q_2, q_3)$

$$\therefore n_P = \frac{(p_1, p_2, p_3)}{\sqrt{p_1^2 + p_2^2 + p_3^2}}; n_Q = \frac{(q_1, q_2, q_3)}{\sqrt{q_1^2 + q_2^2 + q_3^2}}$$

$$(Q - P) = (q_1 - p_1, q_2 - p_2, q_3 - p_3)$$

$$(P - Q) = (p_1 - q_1, p_2 - q_2, p_3 - q_3)$$

<sup>4</sup> Referred to **Appendix 9.1**

<sup>5</sup> Referred to **Appendix 9.6**

therefore, we can write

$$[(Q - P) \cdot n_P][(P - Q) \cdot n_Q] = [(Q - P) \cdot (P - Q)][n_P \cdot n_Q]$$

which leads to

$$[(q_1 - p_1, q_2 - p_2, q_3 - p_3) \cdot (p_1 - q_1, p_2 - q_2, p_3 - q_3)][n_P \cdot n_Q]$$

therefore  $[(Q - P) \cdot n_P][(P - Q) \cdot n_Q] = -[(p_1 - q_1)^2 + (p_2 - q_2)^2 + (p_3 - q_3)^2] [n_P \cdot n_Q]$

where  $n_P \cdot n_Q$  is the dot product and so it would give a constant.

$$n_P \cdot n_Q = \frac{(p_1, p_2, p_3)}{\sqrt{p_1^2 + p_2^2 + p_3^2}} \cdot \frac{(q_1, q_2, q_3)}{\sqrt{q_1^2 + q_2^2 + q_3^2}} = \frac{p_1 q_1 + p_2 q_2 + p_3 q_3}{\sqrt{(p_1^2 + p_2^2 + p_3^2)(q_1^2 + q_2^2 + q_3^2)}}$$

on the other side,  $|P - Q| = \sqrt{(p_1 - q_1)^2 + (p_2 - q_2)^2 + (p_3 - q_3)^2}$

$$\therefore |P - Q|^4 = [(p_1 - q_1)^2 + (p_2 - q_2)^2 + (p_3 - q_3)^2]^2$$

$$\begin{aligned} \therefore \frac{[(Q - P) \cdot n_P][(P - Q) \cdot n_Q]}{|P - Q|^4} &= \frac{-[(p_1 - q_1)^2 + (p_2 - q_2)^2 + (p_3 - q_3)^2][n_P \cdot n_Q]}{[(p_1 - q_1)^2 + (p_2 - q_2)^2 + (p_3 - q_3)^2]^2} \\ &= \frac{-[n_P \cdot n_Q]}{(p_1 - q_1)^2 + (p_2 - q_2)^2 + (p_3 - q_3)^2} \quad \blacksquare \end{aligned}$$

As the Kernel G-function is defined above,  $u(Q)$  is eliminated in the integration of  $u(P) - u(Q)$

with respect to  $Q$  and so the Kernel G-function is proved to be weakly-singular. Since the

brightness function,  $u(P)$ , is what we need to find from the Radiosity model, under the condition

that G is a weakly-singular function, we are unable to integrate this directly. We are however

capable of finding the solution numerically.

## 2 Galerkin Method

Since the Radiosity model is proved to be a Fredholm integral equation of the second kind with a weakly singular kernel (from the previous section), it's impossible to evaluate this integral analytically. Several integral methods can be used to find the solutions of integral equations, such as “the Adomian Decomposition Method”<sup>6</sup> and “the Modified Decomposition Method”<sup>7</sup>. However, these methods cannot be used for this project because they are not numerical methods, and therefore would not provide numerical solutions.

The Galerkin Method<sup>8</sup> is a numerical method used to convert a continuous operator problem (such as a partial differential equation) to a discrete problem in a weak formulation. The approach is credited to Boris Grigoryevich Galerkin but the method was discovered by Walther Ritz.<sup>9</sup> It is one of the most common method of calculating the global stiffness matrix in the Finite-Element method. The Galerkin Method of weighted residuals can not only solve weakly-singular/non-weakly-singular Fredholm integral equations<sup>10</sup>, but also overcome the non-uniqueness problem arising in integral equation. Therefore, the Galerkin Method of weighted residuals is used in our research.

### 2.1 Finite-Element Method<sup>11</sup>

The Finite-Element method is a variational technique to approximate the solution of two-point boundary-value problem for partial differential equations. In the real-life situation, most of applied mathematical problems have boundary conditions involving derivatives and irregularly shaped boundaries. Each boundary condition involving a derivative is required to be

---

<sup>6</sup> Referred to **Appendix 9.3**

<sup>7</sup> Referred to **Appendix 9.4**

<sup>8</sup> Referred to **Appendix 9.2**

<sup>9</sup> Galerkin Method <[https://en.wikipedia.org/wiki/Galerkin\\_method](https://en.wikipedia.org/wiki/Galerkin_method)>

<sup>10</sup> Referred to **Appendix 9.7**

<sup>11</sup> Ref [5]. Pg 696 and Pg 746

approximated by a difference quotient at the grid points, and the irregularly shaped boundary makes it more difficult to place the grid points. The Finite-Element method can minimize a certain integral, in which the original boundary-value problem would be reformulated as a problem, bounded by the set of sufficiently differentiable functions satisfying the boundary conditions. The Galerkin Method of weighted residuals used in our research is derived from the Finite-Element Method.

## ***2.2 Method of Mean Weighted Residuals<sup>12</sup>***

When the Method of Mean Weighted Residuals is applied to solve a partial differential equation numerically, the solution of this partial differential equation is assumed to be well approximated by a finite sum of test functions. The method is used to find the coefficient value of each corresponding test function. The resulting coefficients are used to minimize the error between the true solution and the linear combination of test functions. The choice of test function depends on the specific method used. The two major elements of the Mean Weighted Residuals Method are inner product of functions and basis of a vector space of functions. In such case, since the Galerkin Method of weighted residuals has been already chosen for the research, the basis functions themselves would be used as test functions to approximate the solution of the Radiosity Model.

## ***2.3 Galerkin Method of Weighted Residuals<sup>13</sup>***

Inner product of two functions in a certain domain has the form:

$$\langle f, g \rangle = \int_a^b f(x)g(x)dx$$

***Equation 2.1*** The form of inner product of Galerkin Method of Weighted Residuals

---

<sup>12</sup> Ref [5]

<sup>13</sup> Ref [6]



which shows the inner product of  $f(x)$  and  $g(x)$  on the interval  $[a, b]$ . Looking at our Radiosity model from **Equation 1.1**, the partial integral contains an inner product of  $u(Q)$  (the brightness at exterior point outside of the surface) and  $G(P, Q)$  (the Kernel term of the integral).

The function space is defined as  $V$ , and the basis of  $V$  is a set of linearly independent functions as:

$$S = \{\phi_j(x)\}_{j=0}^{\infty}$$

**Equation 2.2** *The set of all basis functions of the Galerkin Method of Weighted Residuals*

therefore, any function  $f(x) \in V$  can be uniquely written as the linear combination of the basis functions as:

$$f(x) = \sum_{j=0}^{\infty} C_j \phi_j(x)$$

**Equation 2.3** *The form of the linear combination of basis functions*

Where  $C_j$  are the coefficients and  $\phi_j(x)$  are the basis functions. There are generally four steps using the Galerkin Method of Weighted Residuals to solve a partial differential equation numerically.<sup>14</sup>

Suppose  $D(U) = 0$  is a differential equation with a boundary  $B(U)$ :

$$D(U) = L(U(x)) + f(x) = 0 \text{ on } B[U] = [a, b]$$

where  $L$  is a differential operator, and  $f$  is a given function.

**Step 1.** Set up a “trial solution” of  $U$ :

$$U \approx u(x) = \phi_0(x) + \sum_{j=1}^n C_j \phi_j(x)$$

then residual is defined as:

---

<sup>14</sup> Ref [17]

$$R(x) = D[u(x)] = L(U(x)) + f(x)$$

**Step 2.** Choose an arbitrary weight function  $w(x)$ , which means:

$$\langle w, R(x) \rangle = \langle w, D(u) \rangle = \int_a^b w(x)\{D[u(x)]\}dx = 0$$

from the theory of orthogonality of inner products:

$$\text{If } \langle f, g \rangle = \int_a^b f(x)g(x)dx = 0$$

Then  $f(x)$  and  $g(x)$  are orthogonal. Therefore, the trial function partially satisfies the problem.

**Step 3.** Choose a weight function  $w$  from the basis functions  $\phi_j$ , then

$$\langle w, R(x) \rangle = \int_a^b \phi_j, \{D[u(x)]\}dx = \int \phi_j(x) \left\{ D \left[ \phi_0(x) + \sum_{j=1}^n C_j \phi_j(x) \right] \right\} dx = 0$$

we have a set of  $n$ -order linear equations. The coefficients  $C_j$  can be obtained by solving the system.

**Step 4.** The trial solution  $u(x) = \phi_0(x) + \sum_{j=1}^n C_j \phi_j(x)$  would be the final approximated solution.

Therefore, in order to apply the Galerkin Method of Weighted Residuals in our own research, we need to define specific boundary and basis function.

## 2.4 Gaussian Quadrature<sup>15</sup>

When a function has no explicit antiderivative or its antiderivative is difficult to obtain, it is quite challenging to evaluate the definite integral of that function. The “numerical quadrature” based on the interpolation polynomials is the basic method to approximate the integral under this

---

<sup>15</sup> Ref [5] Pg 746

situation. The basic idea is to select a set of distinct nodes  $\{x_0, x_1, \dots, x_n\}$  from the interval  $[a, b]$ .

The Lagrange interpolating polynomial would be integrated as:

$$P_n(x) = \sum_{i=0}^n f(x_i)L_i(x)$$

**Equation 2.4** *The form of the Lagrange interpolating polynomial*

The quadrature formula is given by:

$$\int_a^b f(x)dx \approx \sum_{i=0}^n a_i f(x_i)$$

**Equation 2.5** *The Quadrature formula*

For the Trapezoidal rule and Simpson's rule<sup>16</sup>, the formula is produced by using the first and second Lagrange polynomials with equally-spaced nodes.

Trapezoidal Rule:

$$\int_a^b f(x)dx = \frac{h}{2}[f(x_0) + f(x_1)] - \frac{h^3}{12}f''(\xi)$$

**Equation 2.6** *The form of the Trapezoidal Rule*

The error term for the Trapezoidal rule involves the second derivative of  $f$ , so it gives exact results when applied to any polynomial of degree one or less.

Simpson's Rule:

$$\int_{x_0}^{x_2} f(x)dx = \frac{h}{3}[f(x_0) + 4f(x_1) + f(x_2)] - \frac{h^5}{90}f^{(4)}(\xi)$$

**Equation 2.7** *The form of the Simpson's Rule*

The error term for the Simpson's rule involves the fourth derivative of  $f$ , so it gives exact results when applied to any polynomial of degree three or less. However, both the Trapezoidal rule and the Simpson's rule and other Newton-Cotes formulas use values of the functions which are

---

<sup>16</sup> Ref [5] Pg 194

equally-spaced. This restriction can significantly decrease the accuracy of the approximation.

Therefore, the Gaussian quadrature is required because it chooses the points for evaluation in an optimal (rather than equally-spaced) way.

An integral  $\int_a^b f(x)dx$  over an arbitrary interval  $[a, b]$  can be transformed into an integral over  $[-1, 1]$  by using the change of variables:

$$t = \frac{2x - a - b}{b - a} \Leftrightarrow x = \frac{1}{2}[(b - a)t + a + b]$$

Then the Gaussian quadrature can be applied to any interval  $[a, b]$  as shown below<sup>17</sup>:

$$\int_a^b f(x)dx = \int_{-1}^1 f\left(\frac{(b - a)t + (b + a)}{2}\right) \frac{(b - a)}{2} dt$$

*Equation 2.8 Change of interval by applying the Gaussian quadrature*

Therefore, the boundary of the Fredholm integral equation of the second kind in the Radiosity Equation can be converted to  $[-1, 1]$  by applying the Gaussian quadrature nodes.

## 2.5 Basis Function

To apply the Galerkin Method of Weighted Residuals in this research, the spherical harmonics function was chosen to be the basis function.<sup>18</sup> Let  $U = \{(x, y, z): x^2 + y^2 + z^2 = 1\}$  be the unit sphere in  $\mathfrak{R}^3$ . If the homogeneous harmonic polynomials of degree  $n$  in  $\mathfrak{R}^3$  are restricted to  $U$ , then their restrictions are called the spherical harmonics of degree  $n$ . If any other polynomial is restricted to  $U$ , then its restriction is called a spherical polynomial. Let  $p_n(U)$  and  $p_n^m(U)$  denote the Legendre polynomials and associated Legendre functions on interval  $[-1, 1]$ , where  $n \geq 0$ , and  $1 \leq m \leq n$ . Then the spherical harmonic functions of degree  $n$  (basic functions) would be given by:

---

<sup>17</sup> Ref [5] Pg 233

<sup>18</sup> Ref [2]

$$p_n(\cos \theta), \quad p_n^m(\cos \theta) \cos(m\phi), \quad p_n^m(\cos \theta) \sin(m\phi)$$

**Equation 2.9** Basis functions: the spherical harmonic functions

Using spherical polynomials to define the approximating subspaces, the Galerkin Method can be applied to the Radiosity Equation. The numerical solution of the brightness at the interior point of the surface is given by:

$$U(P) = \sum_{j=1}^d a_j h_j$$

**Equation 2.10** The form of the general solution for the Radiosity Equation by the Galerkin Method

$$\text{where } a_j(h_j, h_i) - \sum_{j=1}^d a_j(Gh_j, h_i) = (E, h_i), \quad i = 1 \dots d$$

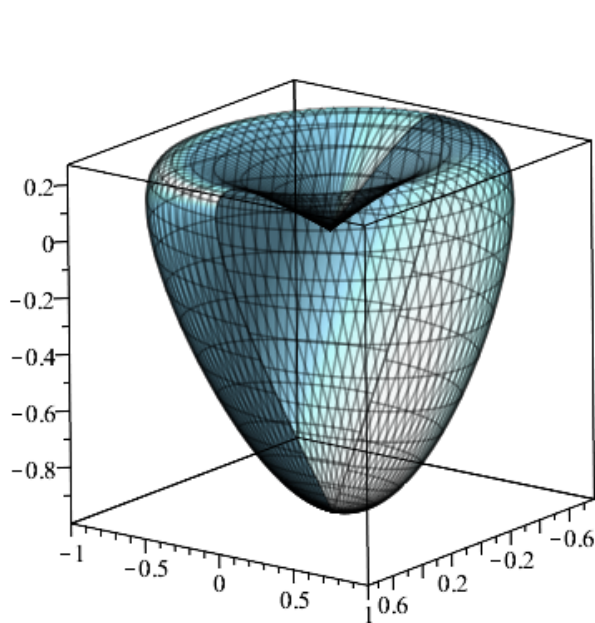
$U(P)$  = Brightness at interior point;  $G$  = Kernel term;  $E$  = Emissivity

The true solution of the Radiosity model was assumed to be  $U(P) = E(P)$ . With the Galerkin coefficients, the convergence errors between the true solutions and the approximated solutions would be calculated using a Fortran 77 program.

### 3 The Spherical Shapes

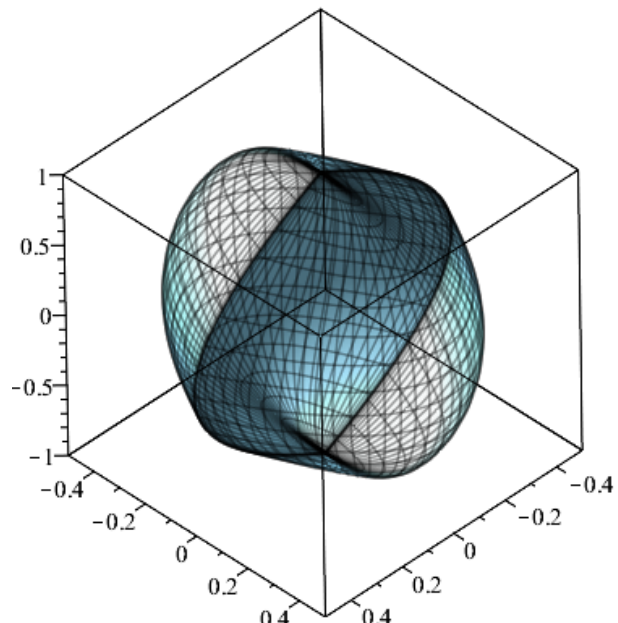
To design a spherical shape for a room in a spacecraft landing on Mars with given Martian emissivity and reflectivity, the spherical shape must be simply connected and closed. It is also necessary to satisfy Green’s Theorem for the application of the Radiosity model. Green’s Theorem states that the value of a double integral over a simply connected region R is determined by the value of a line integral around the boundary of R. Under these requirements for spherical shapes, two shapes were initially designed and studied in this research.

The images of the two shapes, named Spherical Cone and Spherical Rhombus respectively, are presented below:



$$\begin{aligned}
 x &= A \cdot \cos(0.5\theta) \sin(\theta) \cos(\phi) \\
 y &= B \cdot \sin(\theta) \sin(\phi) \\
 z &= C \cdot \sin(0.5\theta) \cos(\theta)
 \end{aligned}$$

**Figure 3.1** Spherical Cone, the first designed shape for studying Radiosity Equation



$$\begin{aligned}
 x &= A \cdot \cos(0.5\theta) \sin(0.5\theta) \sin(\theta) \cos(\phi) \\
 y &= B \cdot \sin(0.5\phi) \sin(0.5\phi) \sin(\theta) \sin(\phi) \\
 z &= C \cdot \cos(\theta)
 \end{aligned}$$

**Figure 3.2** Spherical Rhombus, the second designed shape for studying Radiosity Equation

Where  $0 \leq \theta \leq \pi$  and  $0 \leq \phi \leq 2\pi$ , and the “A”, “B” and “C” are constant coefficients. In this case, we set all coefficients to be 1 for further calculations. The figures were graphed by Maple

17. The two spherical shapes are developed based on the sphere in spherical coordinate system as shown below:

$$x = r \sin \theta \cos \phi$$

$$y = r \sin \theta \sin \phi$$

$$z = r \cos \theta$$

Where  $r$  is the radius,  $\theta$  is the polar angle from the positive  $z$ -axis with  $0 \leq \theta \leq \pi$ , and  $\phi$  is the azimuthal angle in the  $x$ - $y$  plane from the  $x$ -axis with  $0 \leq \phi \leq 2\pi$ . The Radiosity model was solved for these two shapes by the Galerkin Method. The numerical results were presented below.

## 4 Numerical Results (Part I)

In general, for numerical analysis a convergence error of  $10^{-5}$  or smaller is acceptable. As we mentioned in section 2, the errors were calculated by the Fortran 77 program. By comparing the errors of different shapes under different degrees and nodes, we determined the better shape for further investigation.

### 4.1 The Errors for Different Degrees and Nodes

When we use the Galerkin Method to solve the Radiosity Equation, we need to select the degree, interior nodes, and exterior nodes. The ranges of degree ( $n$ ), interior nodes, and exterior nodes are given by:

$$n = \langle 3,5,7 \rangle; \text{ Interior nodes} = \langle 16,32 \rangle; \text{ Exterior nodes} = \langle 8,16,20 \rangle$$

In order to have the absolute errors as small as possible, we tested all the combinations under the given range of degrees and nodes. The reflectivity value was set to be 0.00001, and the emissivity function was 1 (a simple constant function). The following three tables present different errors under different degrees and nodes.

**Table 4.1** Using the Galerkin Method, convergence errors were calculated for five random points. Interior nodes were defaulted to 16, and exterior nodes were defaulted to 8. The value of the degree of the boundary function varied from 3 to 7.

	Degree	(500, 200, 300)	(50, 200, 300)	(500, 20, 300)	(500, 200, 30)	(-4000, -5000, -6000)
Spherical Cone	3	$1.562 \times 10^{-6}$	$1.564 \times 10^{-6}$	$1.561 \times 10^{-6}$	$1.533 \times 10^{-6}$	$1.569 \times 10^{-6}$
	5	$6.205 \times 10^{-7}$	$6.232 \times 10^{-7}$	$6.201 \times 10^{-7}$	$5.918 \times 10^{-7}$	$6.277 \times 10^{-7}$
	7	$9.811 \times 10^{-7}$	$9.784 \times 10^{-7}$	$9.814 \times 10^{-7}$	$1.009 \times 10^{-6}$	$9.739 \times 10^{-7}$
Spherical Rhombus	3	$1.525 \times 10^{-6}$	$1.528 \times 10^{-6}$	$1.524 \times 10^{-6}$	$1.533 \times 10^{-6}$	$1.525 \times 10^{-6}$
	5	$5.843 \times 10^{-7}$	$5.870 \times 10^{-7}$	$5.837 \times 10^{-7}$	$5.922 \times 10^{-7}$	$5.844 \times 10^{-7}$
	7	$1.017 \times 10^{-6}$	$1.015 \times 10^{-6}$	$1.018 \times 10^{-6}$	$1.009 \times 10^{-6}$	$1.017 \times 10^{-6}$



**Table 4.1**, shows that for both spherical shapes, the Galerkin Method of degree 5 gave the smallest errors compared to the results of other two degrees. Therefore, the degree of 5 was chosen for the Galerkin Method to calculate errors. We needed to further investigate the best values of interior nodes and exterior nodes.

**Table 4.2** Using the Galerkin Method, convergence errors were calculated for five random points. The degree was set to be 5, and exterior nodes were defaulted to 8. The values of interior nodes varied from 16 to 32.

	Interior Node	(500, 200, 300)	(50, 200, 300)	(500, 20, 300)	(500, 200, 30)	(-4000, -5000, -6000)
Spherical Cone	16	$6.205 \times 10^{-7}$	$6.232 \times 10^{-7}$	$6.201 \times 10^{-7}$	$5.918 \times 10^{-7}$	$6.277 \times 10^{-7}$
	32	$7.477 \times 10^{-7}$	$7.487 \times 10^{-7}$	$7.477 \times 10^{-7}$	$7.400 \times 10^{-7}$	$7.498 \times 10^{-7}$
Spherical Rhombus	16	$5.843 \times 10^{-7}$	$5.870 \times 10^{-7}$	$5.837 \times 10^{-7}$	$5.922 \times 10^{-7}$	$5.844 \times 10^{-7}$
	32	$7.411 \times 10^{-7}$	$7.414 \times 10^{-7}$	$7.410 \times 10^{-7}$	$7.421 \times 10^{-7}$	$7.411 \times 10^{-7}$

Since there were only two options for the interior nodes, it was apparent that the errors for interior nodes at 16 were smaller than those of interior nodes at 32. Therefore, we chose the interior node to be 16, and continued to test for the exterior nodes.

**Table 4.3** Using the Galerkin Method, convergence errors were calculated for five random points. The degree was set to be 5, and the interior nodes were set to be 16. The values of exterior nodes varied from 8 to 20.

	Exterior Node	(500, 200, 300)	(50, 200, 300)	(500, 20, 300)	(500, 200, 30)	(-4000, -5000, -6000)
Spherical Cone	8	$6.205 \times 10^{-7}$	$6.232 \times 10^{-7}$	$6.201 \times 10^{-7}$	$5.918 \times 10^{-7}$	$6.277 \times 10^{-7}$
	16	$6.205 \times 10^{-7}$	$6.233 \times 10^{-7}$	$6.203 \times 10^{-7}$	$5.923 \times 10^{-7}$	$6.277 \times 10^{-7}$
	20	$6.206 \times 10^{-7}$	$6.233 \times 10^{-7}$	$6.203 \times 10^{-7}$	$5.924 \times 10^{-7}$	$6.277 \times 10^{-7}$
Spherical Rhombus	8	$5.843 \times 10^{-7}$	$5.870 \times 10^{-7}$	$5.837 \times 10^{-7}$	$5.922 \times 10^{-7}$	$5.844 \times 10^{-7}$
	16	$5.844 \times 10^{-7}$	$5.871 \times 10^{-7}$	$5.838 \times 10^{-7}$	$5.923 \times 10^{-7}$	$5.844 \times 10^{-7}$
	20	$5.843 \times 10^{-7}$	$5.870 \times 10^{-7}$	$5.838 \times 10^{-7}$	$5.924 \times 10^{-7}$	$5.845 \times 10^{-7}$

In **Table 4.3**, the errors calculated under three different exterior nodes were very close to each other. However, the errors for the exterior nodes at 8 were a little smaller (difference within  $10^{-7}$

<sup>10</sup>) than those of other two exterior nodes. Although the difference among three exterior nodes was extremely small, the exterior node at 8 was still better than the other two nodes. Therefore, after testing all the degrees and nodes, the degree of 5, interior node at 16, and exterior node at 8 were the best combination for the Galerkin Method to solve Radiosity Equation on Spherical Cone and Spherical Rhombus.

#### 4.2 The Errors of the Two Spherical Shapes

Under the degree of 5, interior node at 16, and exterior node at 8, the errors between the approximated solution and true solution for two spherical shapes were calculated by Fortran 77 program. The emissivity function was set to be 1. The reflectivity values ranged from  $5 \times 10^{-5}$  to  $4 \times 10^{-7}$ , therefore, we could obtain how the change of reflectivity values affected the convergence errors.

**Table 4.4** Using the Galerkin Method, convergence errors were calculated for five random points with different reflectivity values ranging from  $5 \times 10^{-5}$  to  $4 \times 10^{-7}$  for the Spherical Cone.

Spherical Cone	Point Coordinate				
Reflectivity	(500, 200, 300)	(50, 200, 300)	(500, 20, 300)	(500, 200, 30)	(-4000, -5000, -6000)
$5 \times 10^{-5}$	$3.102 \times 10^{-6}$	$3.122 \times 10^{-6}$	$3.102 \times 10^{-6}$	$2.958 \times 10^{-6}$	$3.140 \times 10^{-6}$
$1 \times 10^{-5}$	$6.205 \times 10^{-7}$	$6.232 \times 10^{-7}$	$6.201 \times 10^{-7}$	$5.918 \times 10^{-7}$	$6.277 \times 10^{-7}$
$3 \times 10^{-6}$	$1.861 \times 10^{-7}$	$1.869 \times 10^{-7}$	$1.861 \times 10^{-7}$	$1.780 \times 10^{-7}$	$1.883 \times 10^{-7}$
$2 \times 10^{-6}$	$1.241 \times 10^{-7}$	$1.249 \times 10^{-7}$	$1.242 \times 10^{-7}$	$1.178 \times 10^{-7}$	$1.262 \times 10^{-7}$
$4 \times 10^{-7}$	$2.480 \times 10^{-8}$	$2.487 \times 10^{-8}$	$2.478 \times 10^{-8}$	$2.372 \times 10^{-8}$	$2.511 \times 10^{-8}$

**Table 4.5** Using the Galerkin Method, convergence errors were calculated for five random points with different reflectivity values ranging from  $8.00 \times 10^{-2}$  to  $1.00 \times 10^{-10}$  for the Spherical Rhombus

Spherical Rhombus	Point Coordinate				
Reflectivity	(500, 200, 300)	(50, 200, 300)	(500, 20, 300)	(500, 200, 30)	(-4000, -5000, -6000)
$5 \times 10^{-5}$	$2.920 \times 10^{-6}$	$2.943 \times 10^{-6}$	$2.920 \times 10^{-6}$	$2.964 \times 10^{-6}$	$2.922 \times 10^{-6}$
$1 \times 10^{-5}$	$5.843 \times 10^{-7}$	$5.870 \times 10^{-7}$	$5.837 \times 10^{-7}$	$5.922 \times 10^{-7}$	$5.844 \times 10^{-7}$
$3 \times 10^{-6}$	$1.751 \times 10^{-7}$	$1.759 \times 10^{-7}$	$1.753 \times 10^{-7}$	$1.772 \times 10^{-7}$	$1.753 \times 10^{-7}$
$2 \times 10^{-6}$	$1.171 \times 10^{-7}$	$1.172 \times 10^{-7}$	$1.158 \times 10^{-7}$	$1.182 \times 10^{-7}$	$1.170 \times 10^{-7}$
$4 \times 10^{-7}$	$2.343 \times 10^{-8}$	$2.351 \times 10^{-8}$	$2.330 \times 10^{-8}$	$2.372 \times 10^{-8}$	$2.339 \times 10^{-8}$

The results (from **Table 4.4** and **Table 4.5**) show that the convergence errors decreased as the reflectivity value decreased for both shapes. Then we assumed that the convergence error to be directly proportional with the value of reflectivity. Since we use the numerical methods to solve our problems, and we cannot evaluate an exact solution, the errors must be as small as possible. From the previous sections, we consider that errors within  $10^{-5}$  or smaller are sufficient and necessary to validate the numerical method. In this case, the convergence errors were within  $10^{-6}$  to  $10^{-8}$  which were small enough for both shapes. To determine which shape gave better results for further research, the convergence errors of two shapes were compared in **Figure 4.1**.

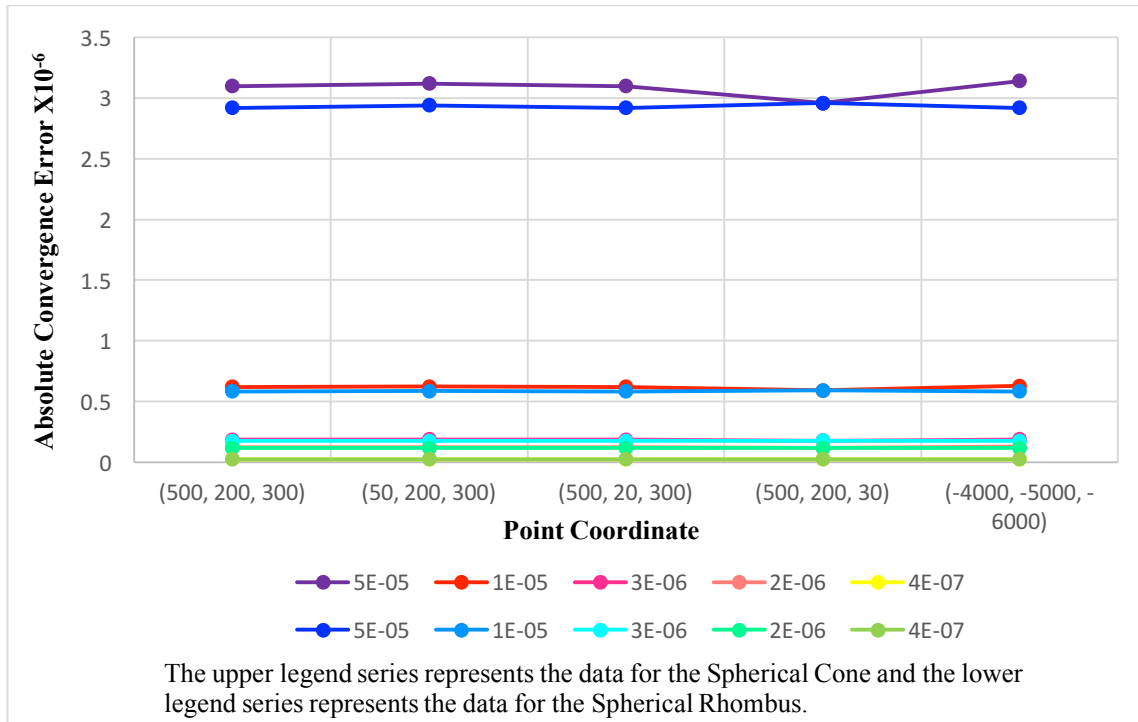


**Figure 4.1** Convergence errors of the Spherical Cone and Spherical Rhombus. The range of reflectivity values varied from  $5.00 \times 10^{-5}$  to  $4.00 \times 10^{-7}$

**Figure 4.1**, shows convergence errors for the Spherical Rhombus are always lower than those of the Spherical Cone, at the same reflectivity values from  $5.00 \times 10^{-5}$  to  $4.00 \times 10^{-7}$ . We can conclude that the Spherical Rhombus (the second shape) produces more reliable results with smaller convergence errors. However, the convergence errors were computed theoretically under the given conditions, where brightness is assumed to be constant and the boundary function for the Radiosity equation is equal to 1. The errors were small enough only for small reflectivity values. To make the design of shape more applicable, we need to further justify the reflectivity to determine how much brightness is required on Mars.

## 5 The Lighting and Brightness for Radiosity

Because the research model for solving the Radiosity Equation is designed to construct an interior space on a spacecraft, and the destination is Mars, it is important to investigate the environment on Mars. The Radiosity is dealing with the energy both emitted from and reflected by a surface, it is necessary to clarify the key terms about reflectivity and emissivity on Mars. On the other hand, as we claimed in the introduction, the requirement of the room design is to achieve the maximum lighting efficiency. It is also necessary to clarify the definition of brightness physically in order to measure the light level inside a room. Since two spherical shapes were tested under a group of extremely small reflectivity values, we need to justify how much brightness is required for different activities.

### 5.1 Mars Background<sup>19</sup>

According to "Mars Background Noise Temperatures", compared with Earth, Mars has lower surface temperatures, much lower atmospheric absorption and radiation, and higher surface emissivity. We are making the assumption that the light source for the interior room of the spacecraft originates from outside of the spacecraft from the Martian atmosphere. Mars has a large surface emissivity due to the land surfaces having lower dielectric constants. No liquid water surface has been detected on Mars. The soil's moisture and surface roughness affect the emissivity, and the color of materials also affects the reflectivity. Earth has lower values of emissivity and reflectivity on average. But, rocks on Mars typically have emissivity less than that of desert sands on Earth. Mars has higher average surface emissivity due to the roughness of soil and rocks on the surface. For any surface maintaining a constant temperature, the incoming energy is the sum of the energy emitted and reflected.

---

<sup>19</sup>Ref [3]

## 5.2 Measuring Light Levels

According to the Autodesk Sustainability Workshop, the “brightness” of light is constituted by three major elements: the amount of light coming from a light source called luminous flux (lumens), the amount of light falling on a surface called illuminance (lux), and the amount of light reflected off a surface called luminance ( $\text{cd}/\text{m}^2$ ).

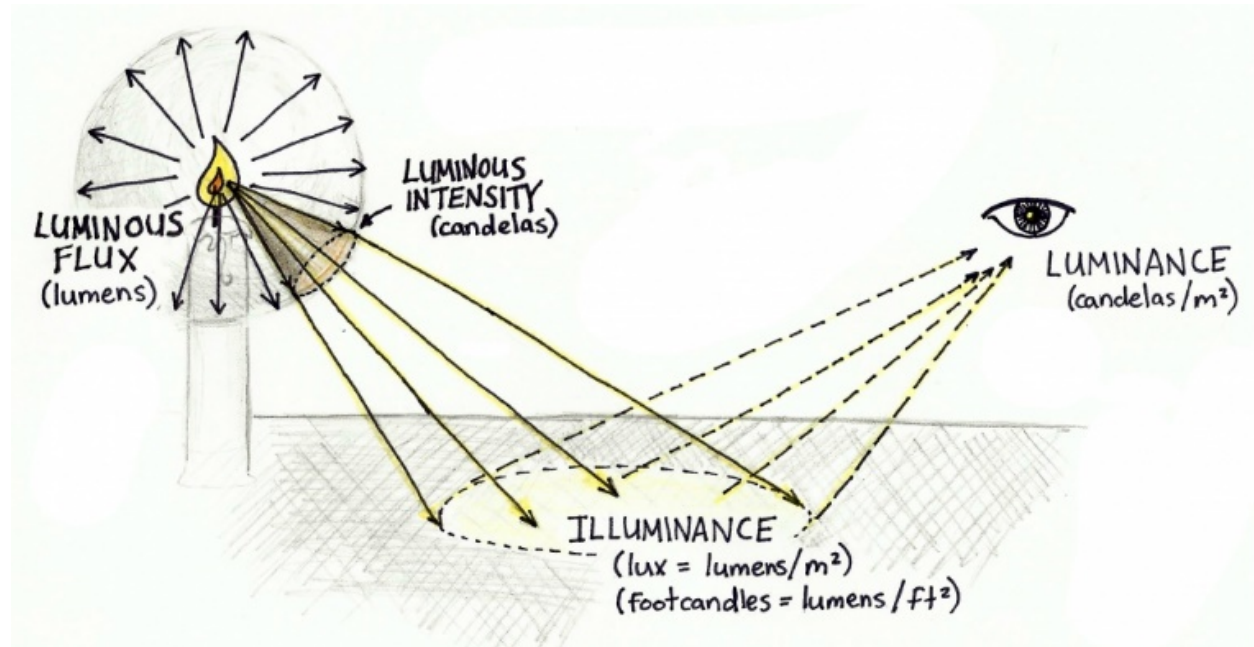


*Figure 5.1 Constitutions of the “brightness” of light<sup>20</sup>*

*Luminous Flux= Light Coming from a Source*

As **Figure 5.1** shows, the luminous flux (also called ‘luminous power’) is a measure of the total perceived power of light. It is measured in lumens, which are a useful metric for describing how bright a light source is. (For a better understanding, consider that the luminous flux of a 60W incandescent light bulb is about 850 lumens)

<sup>20</sup> The Autodesk Sustainability Workshop, Measuring Light Levels

*Illuminance= Light Falling on a Surface*

The illuminance is measured in lux which is a metric unit as lumens/m<sup>2</sup>. Because illuminance measures the amount of light falling on a surface within a certain area, it does not depend on the material properties of the surface being illuminated. However, the amount of light on the surface, which can be visualized, does depend on how much is being reflected from other surfaces around it. Therefore, the value of illuminance is dependent on the color and reflectance of the surrounding surfaces. The brightness of the sky is measured using illuminance on unobstructed horizontal planes. The table below lists some common illumination levels, which represent the total illumination available from the sky. For our project, we used the illuminance of 10000 lumens/m<sup>2</sup>. Because we cannot guarantee the real illumination available one Mars, we just currently pick an appropriate number based on **Table 5.1** for this research.

*Table 5.1 Common illumination levels available from the Engineering Toolbox*

Condition	Lux (lumens/m <sup>2</sup> )
Full Daylight	10752
Overcast Day	1075
Very Dark Day	107
Twilight	10.8
Deep Twilight	1.08
Full Moon	0.108
Quarter Moon	0.0108
Starlight	0.0011

*Luminance= Light Reflected by a Surface*

Luminance is the light reflected by surfaces and measured in candelas per square meter (cd/m<sup>2</sup>).

The candela presents the luminous flux per unit solid angle reflected by a point light source in a

particular direction. It is the amount of light which would be perceived by human eyes.

Therefore, the quality and intensity of the light does depend on the material properties of the surfaces such as color, reflectance and texture.

Since we use the reflectivity value at  $1.00 \times 10^{-5}$ , from **Table 5.1** assuming the illumination during the daylight on Mars is 10000 lux, the amount of 0.1 lux only would be reflected by the surface on the spacecraft landing on Mars. Although the requirement of the room shape design is to achieve the maximum lighting efficiency, it is important for astronauts to have enough brightness for their activity inside a spacecraft. **Table 5.2** shows the recommended light levels for different activities.

*Table 5.2 Recommended light levels for different activities from the illuminating Engineering Society*

Standard Maintained Illuminance (lux)	Characteristics of Activity	Representative Activity
50	Interiors rarely used for visual tasks (no perception of detail)	Cable tunnels, nighttime sidewalk, parking lots
100 - 150	Interiors with minimal demand for visual acuity (limited perception of detail)	Corridors, changing rooms, loading bay
200	Interiors with low demand for visual acuity (some perception of detail)	Foyers and entrances, dining rooms, warehouses, restrooms
300	Interior with some demand for visual acuity (frequently occupied spaces)	Libraries, sports and assembly halls, teaching spaces, lecture theaters
500	Interior with moderate demand for visual acuity (some low contrast, color judgment tasks)	Computer work, reading & writing, general offices, retail shops, kitchens
750	Interior with demand for good visual acuity (good color judgment, inviting interior)	Drawing offices, chain stores, general electronics work



According to the data from the table above, it requires illuminance at 50 lux at least for the basic activity (interiors rarely used for visual tasks). Therefore, the illuminance of 0.1 lux is completely unrealistic with the reflectivity value less than  $1.00 \times 10^{-5}$ . To satisfy the lowest standard maintained illuminance (50 lux), with assumed illumination on Mars is 10000 lux, the reflectivity value needs to be at least  $(50/10000 =) 0.005$ . Therefore, we need to further research how large the convergence errors of two spherical shapes would be, when the reflectivity value increased to 0.005 at least.

## 6 Realistic Applications

### 6.1 The Errors of the Two Spherical Shapes for Practical Reflectivity Values

From the section of numerical results (part I), both spherical shapes gave small errors under the reflectivity values varying from  $5 \times 10^{-5}$  to  $4 \times 10^{-7}$ . We need to test if both shapes would still give small enough errors if the reflectivity value becomes more realistic. The following table presents the errors of two shapes for the reflectivity value at 0.005. The degrees, nodes, and emissivity function all remain the same as before.

**Table 6.1** the convergence errors of two spherical shapes when the reflectivity values were set to be 0.005.

	Point Coordinate				
Reflectivity = 0.005	(500, 200, 300)	(50, 200, 300)	(500, 20, 300)	(500, 200, 30)	(-4000, -5000, -6000)
Spherical Cone	$1.215 \times 10^{-4}$	$1.223 \times 10^{-4}$	$1.220 \times 10^{-4}$	$1.192 \times 10^{-4}$	$1.228 \times 10^{-4}$
Spherical Rhombus	$1.204 \times 10^{-4}$	$1.201 \times 10^{-4}$	$1.198 \times 10^{-4}$	$1.203 \times 10^{-4}$	$1.198 \times 10^{-4}$

**Table 6.1**, shows that the errors for both shapes became much larger under a constant emissivity function and a realistic value for reflectivity. The errors became worse when the emissivity functions become more realistic (not being a constant function). Therefore, we consider that the Galerkin method might not be appropriate for these two spherical shapes to be applied.

Based on the study of previous spherical shapes, the third one named Spherical Pyramid was developed and further researched.

### 6.2 Final Shape: Spherical Pyramid

Under the same requirements from previous section (3 The Spherical Shapes) for spherical shapes, after several numerical tests and investigation, the spherical pyramid was chosen.

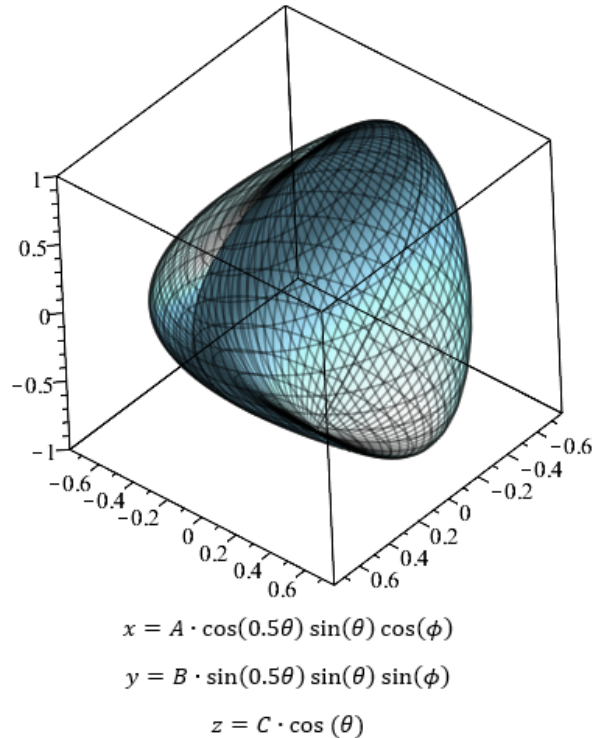


**Figure 6.1** Spherical Pyramid, the third designed shape for studying the Radiosity Model

Where  $0 \leq \theta \leq \pi$  and  $0 \leq \phi \leq 2\pi$ , and the “A”, “B” and “C” are constant coefficients. In this case, we initially set all coefficients to be 1 for further calculations. The coefficients might be changed if we could get better numerical results. The shape was proved to be closed and bounded<sup>21</sup>, and the Green’s Theorem was applied. Different from section 4 Numerical Results (part I), two spherical shapes were tested with one constant emissivity function and various reflectivity values. The Spherical Pyramid will be tested with two reflectivity values (larger than the previous section) and various emissivity functions, which are more realistic to be applied in real life situations, such as sine wave functions, cosine wave functions, and other wave functions.

### **6.3 Consideration of Coordinate Point on Mars**

Because we consider the sunlight is the only light source in our research, it is important to determine how the brightness might change due to different atmospheric layers on Mars.

<sup>21</sup> The complete proof is shown in **Appendix 9.5**

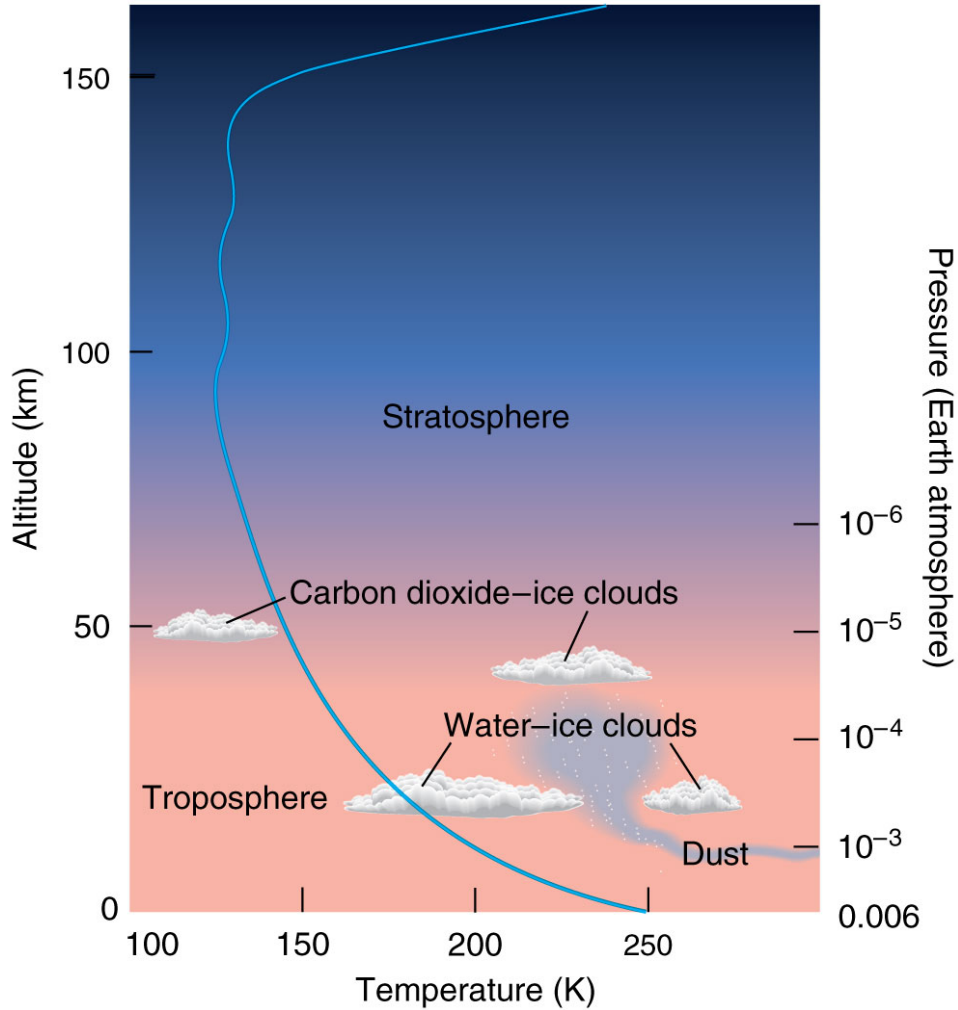
However, we cannot guarantee that the data used in our research is absolutely correct because we are unable to get enough valid information about Martian atmosphere layers from NASA. The data are provided in **Table 6.2**. We believe there must be something in common between atmosphere layers of Mars and Earth, and we will further investigate about Martian atmosphere layers in the future.

**Table 6.2** *The distance of different atmospheric layers from Earth and Mars<sup>22</sup>*

Atmosphere Layers on Earth	Distance (km)	Atmosphere Layers on Mars	Distance (km)
Exosphere	700- 10000		
Thermosphere	80- 700	Stratosphere	$\geq 80$
Mesosphere	50- 80	Carbon dioxide-ice clouds	50- 80
Stratosphere	12- 50	Water-ice clouds	10- 50
Troposphere	$\leq 12$	Troposphere	$\leq 10$

---

<sup>22</sup> Atmosphere of Mars. Encyclopedia of Science. The World of David Darling.



© 2011 Pearson Education, Inc.

**Figure 6.2** Atmospheric layers on Mars<sup>23</sup>

Therefore, according to the distance of different atmospheric layers on Earth, the corresponding coordinate points are set in the following table considering different directions, and distance is calculated from each point to the origin point in units of km. Instead of using random coordinate points, the Spherical Pyramid would be tested under these four specific points.

**Table 6.3** The coordinate points corresponding to the Earth atmospheric layers, the unit of distance is km

Coordinate Point	(3000,4000,5000)	(-10000, -20000, -30000)	(-30000,40000, -50000)	(100000,200000, -300000)
Distance	7.071	37.416	70.711	374.166

<sup>23</sup> The World of David Darling <<http://www.daviddarling.info/encyclopedia/M/Marsatmos.html>>

We wondered if the brightness inside the spacecraft would change or not, when the outside light source came from different atmospheric layers. Because Mars has less atmospheric layers than Earth, we considered the coordinate points only for the first four layers of Earth.

#### 6.4 The Errors under Larger Reflectivity Values

The convergence errors were calculated using the same method as before under reflectivity values of 0.001 and 0.0005, which we consider to be more realistic for random distances.

Different true functions representing the function of emissivity are listed in the following table.

**Table 6.4** Using the Galerkin Method (degree of 5), convergence errors were calculated for four random distances with different reflectivity values (0.001 and 0.0005) and three emissivity functions (also called True Function) for the Spherical Pyramid.

Spherical Pyramid	True Function	Distance from the Center of the Shape (km)			
		7.071	37.416	70.711	374.166
$\rho = 0.001$	1.00	$4.697 \times 10^{-5}$	$4.672 \times 10^{-5}$	$4.675 \times 10^{-5}$	$4.663 \times 10^{-5}$
	$0.001 \sin(0.0001x)$	$4.414 \times 10^{-5}$	$4.344 \times 10^{-5}$	$4.144 \times 10^{-5}$	$3.444 \times 10^{-5}$
	$0.01 \sin(0.0001x)$	$4.174 \times 10^{-5}$	$3.474 \times 10^{-5}$	$1.474 \times 10^{-5}$	$5.526 \times 10^{-5}$
$\rho = 0.0005$	1.00	$2.348 \times 10^{-5}$	$2.336 \times 10^{-5}$	$2.337 \times 10^{-5}$	$2.332 \times 10^{-5}$
	$0.001 \sin(0.0001x)$	$2.194 \times 10^{-5}$	$2.124 \times 10^{-5}$	$1.924 \times 10^{-5}$	$1.224 \times 10^{-5}$
	$0.01 \sin(0.0001x)$	$1.953 \times 10^{-5}$	$1.253 \times 10^{-5}$	$7.465 \times 10^{-5}$	$7.746 \times 10^{-5}$

According to results from **Table 6.4**, the convergence errors for Spherical Pyramid were acceptable within  $10^{-5}$  even though the reflectivity values increased to 0.0005 and 0.001. It is even better that the Spherical Pyramid gives small convergence results under not only constant emissivity functions but also sine wave functions. The previous results for previous shapes gave small errors with constant emissivity functions only, which means the third shape gave much better convergence results for our numerical method. The change of the errors are presented in the following graph.

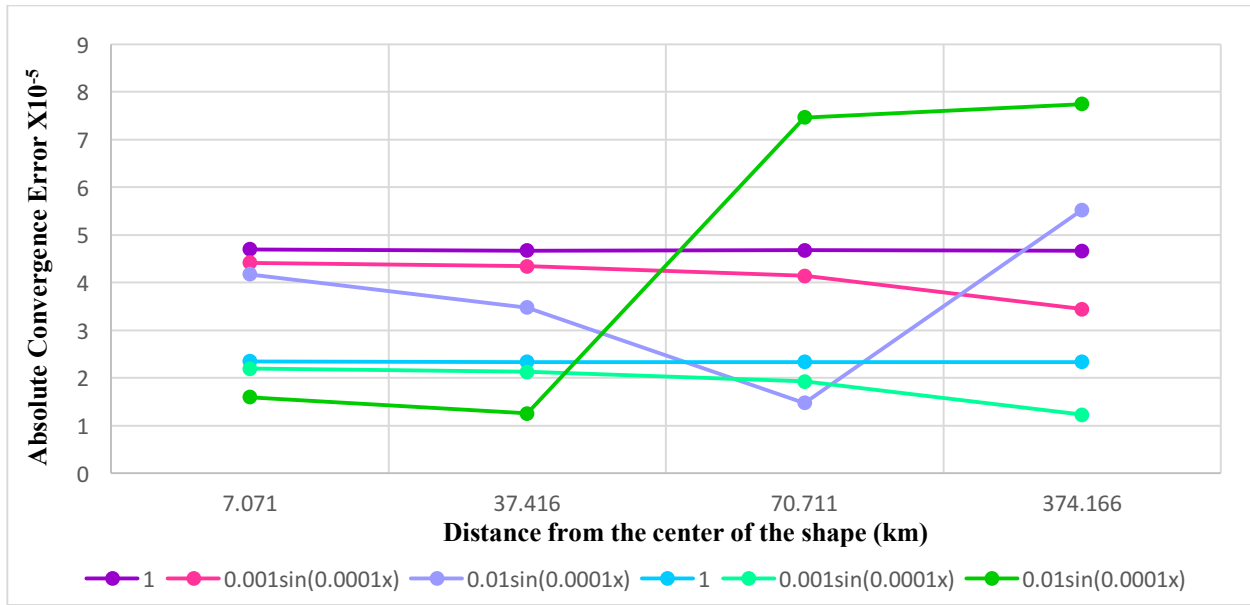


**Figure 6.3** Convergence errors of the Spherical Pyramid with different emissivity functions. Shades of purple represent errors for the reflectivity value of 0.001, and shades of green represent errors for the reflectivity value of 0.0005.

Back to the section about luminous flux, the current reflectivity value is 0.001 which means 10 lux of brightness would be reflected completely by the surface without considering the color, reflectance and texture. However, there still exists a gap between 10 lux and 50 lux (required light level for the basic activity). Therefore, we will further investigate how much the errors would change if the reflectivity is 0.005 (which means the light level for the basic activity would be satisfied at  $\rho = 0.005$ ).

### 6.5 Consideration of Emissivity Functions (True Functions)

In section 7.3, the atmospheric layers on Mars are quite similar with those on Earth. For the time being we assume that the sunlight on Mars has the same illumination as on earth during the daytime. However, there is no standard form for the emissivity function on Mars. Therefore, we considered the sine wave function and the cosine wave function to be the emissivity function for our research.

$$y(t) = A \sin(\omega t + \varphi)$$

**Equation 6.1** The basic form of the sine wave function<sup>24</sup>

$A$  = the amplitude, the peak deviation of the function from zero.

$\omega$  = the angular frequency, the rate of change of the function argument in units of radians per second.

$\varphi$  = the phase (we assume it is 0)

Based on the basic form of the sine wave function, the following emissivity functions were graphed with corresponding equation.

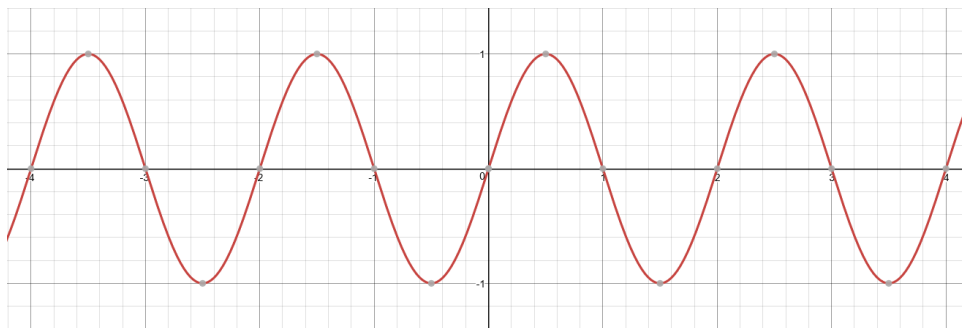


**Figure 6.4**  $\varepsilon = \sin(\pi x)$

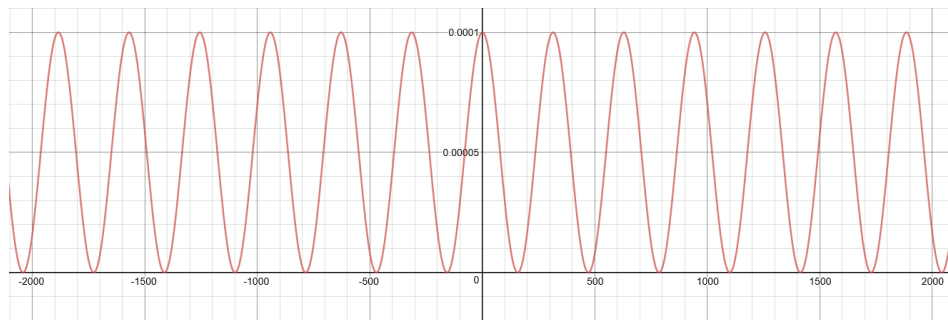


**Figure 6.5**  $\varepsilon = 0.0001\cos^2(0.01x)$

<sup>24</sup> Sine wave [https://en.wikipedia.org/wiki/Sine\\_wave](https://en.wikipedia.org/wiki/Sine_wave)



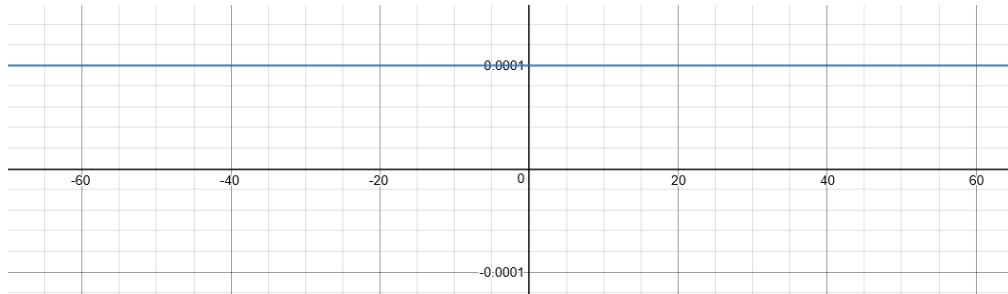


**Figure 6.6**  $\varepsilon = 0.0001\cos^2(0.01x) + 0.0001\sin^2(0.01x)$

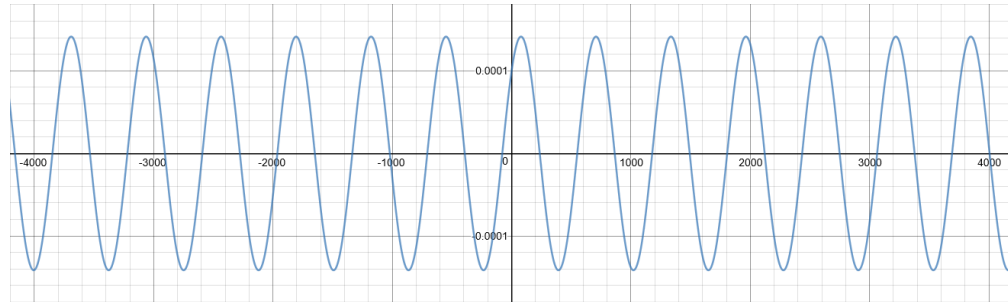


**Figure 6.7**  $\varepsilon = 0.0001 \sin(x) + 0.0001\cos(x)$

We considered these four emissivity functions to be more realistic on the Martian surface rather than a constant function. **Figure 6.6** is a constant function, but we want to compare if the errors would be different between a straight constant function and a sine wave function. We will use these emissivity functions to test if the Spherical Pyramid would still give small enough errors when the reflectivity value increases to 0.005. The following table presents the errors of the Spherical Pyramid when the reflectivity is 0.005

**Table 6.5** Using the Galerkin Method (degree of 5), convergence errors were calculated for four random distances with reflectivity values at 0.005 and five emissivity functions (also called True Function) for the Spherical Pyramid.

Spherical Pyramid	True Function	Distance from the Center of the Shape (km)			
		7.071	37.416	70.711	374.166
$\rho = 0.005$	1.00	$4.672 \times 10^{-4}$	$4.662 \times 10^{-4}$	$4.672 \times 10^{-4}$	$4.662 \times 10^{-4}$
	$\sin(\pi x)$	$4.441 \times 10^{-4}$	$4.441 \times 10^{-4}$	$4.441 \times 10^{-4}$	$4.441 \times 10^{-4}$
	$0.0001 \cos^2(0.01x)$	$4.442 \times 10^{-4}$	$4.451 \times 10^{-4}$	$4.528 \times 10^{-4}$	$5.149 \times 10^{-4}$
	$0.0001 \cos^2(x) + 0.0001 \sin^2(x)$	$4.441 \times 10^{-4}$	$4.441 \times 10^{-4}$	$4.441 \times 10^{-4}$	$4.441 \times 10^{-4}$
	$0.0001 \sin(x) + 0.0001 \cos(x)$	$6.526 \times 10^{-4}$	$7.061 \times 10^{-4}$	$6.511 \times 10^{-4}$	$5.321 \times 10^{-4}$

The results were dissatisfactory. When the reflectivity values increased to 0.005, the errors also increased to  $10^{-4}$ . None of the errors from the table above was within  $10^{-5}$ . Therefore, the shape needed to be improved or we might need a new shape.

### 6.6 The Revised Spherical Pyramid

The three coefficients ( $A, B, C$ ) of  $(x, y, z)$  were set equal to 1 previously. At this point, we reset  $A$  and  $B$  equal to 1.42857, and  $C$  was maintained as 1. The change of the shape is shown below:

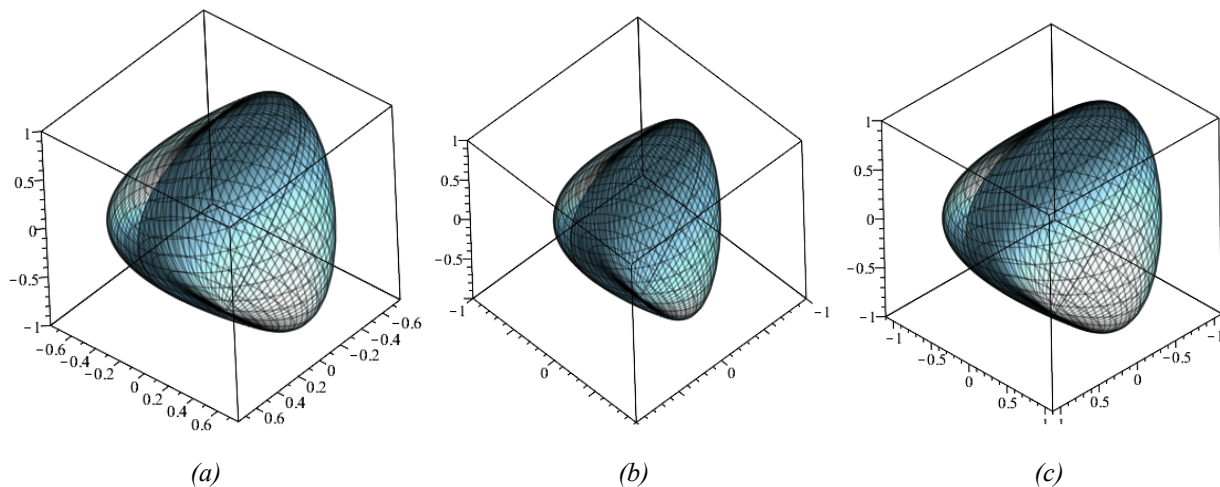


**Figure 6.8** The change of the Spherical Pyramid caused by the change of coefficients

Comparing the three shapes in **Figure 6.8**, figure (a) and figure (b) have the same coefficients, which were equal to one, but had different axis for viewing. We observed that the previous ratio of the ranges in three directions ( $x, y, z$ ) was approximately 0.7: 0.7: 1, and the current ratio is 1: 1: 1. The revised shape (**Figure 6.8** (c)) became more spherical than the previous one, which we expected to give smaller errors.

### 6.7 The Numerical Results (Part III)

Before testing the new revised shape with the reflectivity value at 0.005, we used the same way (section Numerical Results Part I) to investigate the best combination of degree and nodes for the Spherical Pyramid. When we calculated the previous errors for the Spherical pyramid, we assumed the combination for the previous shapes to be the same for the Spherical pyramid. However, we found that the degree of 7, interior node at 16, and exterior node at 8 were the best combination for the Galerkin Method to solve Radiosity model on Spherical Pyramid. Therefore, we used the degree of 7 to recalculate the errors, and the numerical results are presented in the following table and graph.

**Table 6.6** Using the Galerkin Method (degree of 7), convergence errors were calculated for four random distances with reflectivity values at 0.01 and five true functions for the Spherical Pyramid.

Spherical Pyramid	True Function	Distance from the Center of the Shape (km)			
		7.071	37.416	70.711	374.166
$\rho = 0.01$	1.00	$7.562 \times 10^{-5}$	$7.657 \times 10^{-5}$	$7.368 \times 10^{-5}$	$7.620 \times 10^{-5}$
	$\sin(\pi x)$	$9.872 \times 10^{-5}$	$9.872 \times 10^{-5}$	$9.872 \times 10^{-5}$	$9.872 \times 10^{-5}$
	$0.0001 \cos^2(0.01x)$	$1.097 \times 10^{-6}$	$7.307 \times 10^{-5}$	$1.233 \times 10^{-6}$	$3.035 \times 10^{-5}$
	$0.0001 \cos^2(x) + 0.0001 \sin^2(x)$	$9.871 \times 10^{-5}$	$9.872 \times 10^{-5}$	$9.871 \times 10^{-5}$	$9.871 \times 10^{-5}$
	$0.0001 \sin(x) + 0.0001 \cos(x)$	$9.895 \times 10^{-5}$	$8.786 \times 10^{-5}$	$2.680 \times 10^{-6}$	$1.197 \times 10^{-5}$

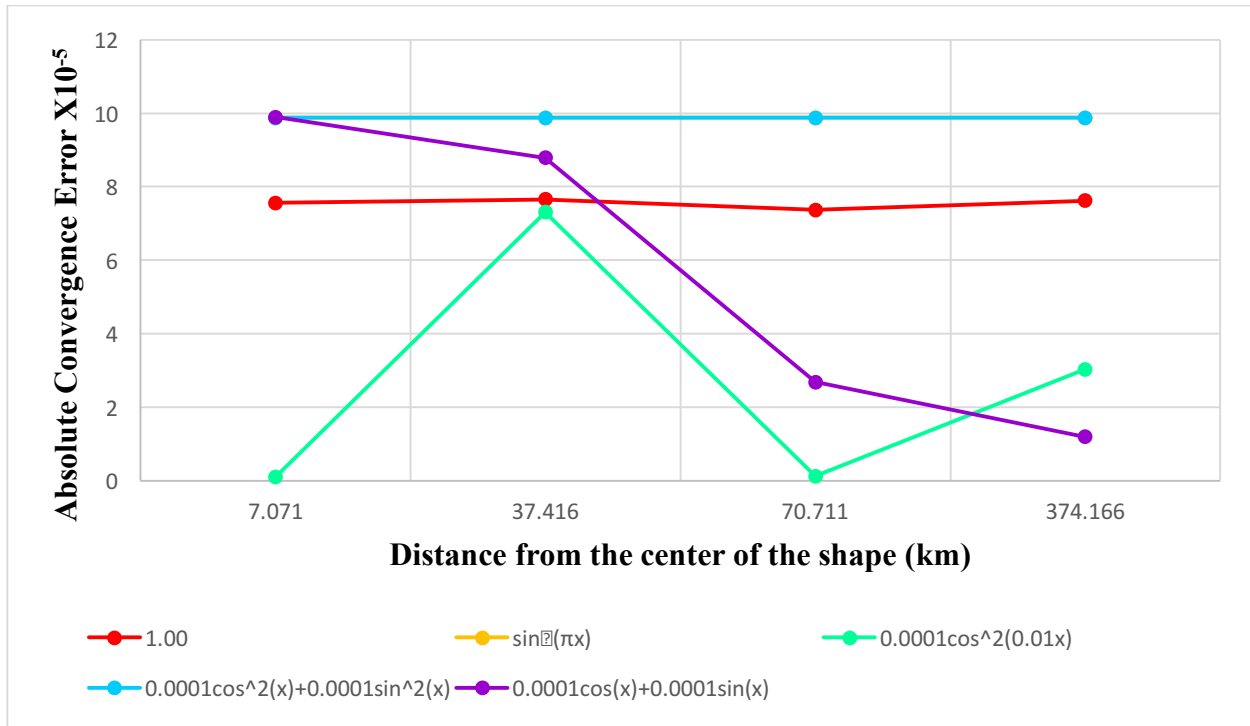


**Figure 6.9** Convergence errors of the Spherical Pyramid with different emissivity functions. The errors of  $\sin(\pi x)$  and  $0.0001 \sin(x) + 0.0001 \cos(x)$  were too close to each other. Therefore, it was difficult to visualize the difference on the graph.

**Table 6.6** shows all the convergence errors were small enough, when the reflectivity value was increased to 0.01. It was quite significant that, not only the reflectivity value of 0.01 was greater than 0.005 (required at least from previous section), but also the reflectivity value of 0.01 was the largest one we could achieve with small enough errors by the time being. As **Figure 6.9** showing, all the errors were within  $10^{-5}$  at least for different emissivity functions, which meant the Spherical Pyramid gave consistent convergence errors for the light coming from different atmospheric layers. When the emissivity function was cosine square, some errors were even within  $10^{-6}$ . The priority for all was that the current reflectivity value increased to 0.01, which presented 100 lux amount of light would be reflected inside Spherical Pyramid. At this point, the brightness inside the shape would be more than 50 lux, so that the spacecraft would have enough illumination, and the light level for basic activity was satisfied on Mars.

## 7 Future Directions/Work

During the entire research, we temporarily consider the brightness from the sunlight on Mars to be the same on Earth. However, the planets do not all receive the same intensity levels of solar energy, due to their different distances from the Sun. The table below presented the information about the relative solar intensity for different planets comparing to the Earth.

*Table 7.1 Relative solar intensity of different planets comparing with the intensity of Earth, due to different distances from the sun only.*<sup>25</sup>

Planet	Mean Distance from Sun (AU)	Relative Solar Intensity
Mercury	0.387	6.680
Venus	0.723	1.913
Earth	1.000	1.000
Mars	1.524	0.431
Jupiter	5.203	0.0369
Saturn	9.539	0.0110
Uranus	19.189	0.00272
Neptune	30.606	0.00111

The relative intensity on Mars was only 0.431 of the intensity on Earth. But, the relative intensity was dependent on the distance from the sun only. The brightness on each planet would also be affected by respective atmospheric layers. Considering the Martian environment and atmosphere, we need to further investigate how much the light intensity exactly can be utilized on the surface of Mars.

On the other side, the Spherical Pyramid gave the good enough results so far when the reflectivity value was 0.01, satisfying the light level for basic activity. We also need to find out

---

<sup>25</sup> Solar Intensity, McAuliffe-Shepard Discovery Center

how much brightness the astronauts might need for different activities. Since the quality and intensity of the light does depend on the material properties of the surfaces such as color, reflectance and texture, we need to further research what materials we could use to build an interior space to satisfy the requirements. The current emissivity functions we used to test the shapes were based on the sine wave function and cosine function. We need to further research more information about real emissivity functions on Mars. Therefore, our spherical shape would be more realistic and applicable as a design for the interior room on a spacecraft that one day might land on Mars.

## 8 References

- [1] Warnapala, Yajni; Deng, Qiuyang. "Numerical Solutions of the Radiosity's Equation for Low Reflectivity and Emissivity on Planet Mars", International Journal of Mathematics Trends and Technology, Vol: 34, ISSN: 2231-5373, Pages: 9-14. 2016. Print.
- [2] Warnapala, Yajni. "Numerical Solution of the Radiosity Equation via Galerkin Method: Dirichlet Condition." International Journal of Numerical Methods and Applications 10 (2013): 73-89. Print.
- [3] Ho, C., S. Slobin, M. Sue, and E. Njoku. "Mars Background Noise Temperatures." IPN Progress Report (2012): 42-149. Web.
- [4] The Autodesk Sustainability Workshop, Measuring Light Levels, <http://sustainabilityworkshop.autodesk.com/buildings/measuring-light-levels>
- [5] Burden, Richard L., and John Douglas. Faires. "Numerical Analysis". Belmont, CA: Thomson Brooks/Cole Cengage Learning, 2011. Print.
- [6] I. O. C. Zienkiewicz, R. L. Taylor, "Finite Element Method", Vol 1, The Basis, 2000
- [7] Wazwaz, Abdul-Majid. *A First Course in Integral Equations*. N.p.: Co.Pte.Ltd. 2015. Print.
- [8] K. E. Atkinson. "The Numerical Solution of Integral Equations of the Second Kind." Cambridge University Press, 1998
- [9] Solar Intensity, McAuliffe-Shepard Discovery Center.  
<<http://www.starhop.com/library/pdf/studyguide/high/brsp-19solarint.pdf>>
- [10] Atmosphere of Mars. Encyclopedia of Science. The World of David Darling. <http://www.daviddarling.info/encyclopedia/M/Marsatmos.html>
- [11] D. C. Catling, C. S. Cockell, and C. P. McKay. "Ultraviolet Radiation on the Surface of Mars" NASA Ames Research Center, Space Science Division/Planetary Systems Branch, Moffett Field, Exobiology Branch, NASA Ames Research Center, Moffett Field.
- [12] K. E. Atkinson and D. Chien. "A study of the fast solution of the occluded Radiosity equation." Electron. Trans. Numer. Anal. 23 (2006), 219-250.
- [13] K. E. Atkinson. "The planar radiosity equation and its numerical solution" Electron. Trans. Numer. Anal. 20 (2000), 303-332.
- [14] T. C. Lin. "The numerical solution of the Helmholtz equation using integral equations." Ph.D. Thesis, University of Iowa, Iowa City, Iowa, 1982.
- [15] A. Voigt, N. Hanssen and C. Weichmann, "The radiosity equation for solving global heat transfer in industrial furnaces" Math. Comput. Model. 39(2-3), 145-150. 2004.
- [16] O. C. Zienkiewicz, R. L. Taylor, Finite Element Method, Vol 1, The Basis, 2000
- [17] Yijian Zhan Ning Ma, Galerkin Method. Computational Engineering

# 9 Appendices

## 9.1 Fredholm Integral Equation of the Second Kind

Fredholm Integral Equation of the Second Kind (Sample Problem)

The equation is defined as  $f(x) - \lambda \int_0^1 9xtf(t)dt = ax^2 - 4x^2$  in space of  $[1, 0]$ :

1) Differentiate both sides of the equation with respect to x:

$$\frac{d}{dx}(f(x) - \lambda \int_0^1 9xtf(t)dt) = f'(x) - \lambda \int_0^1 9tf(t)dt;$$

$$\frac{d}{dx}(ax^2 - 4x^2) = 2ax - 8x;$$

$$\implies f'(x) - \lambda \int_0^1 9tf(t)dt = 2ax - 8x;$$

$$f'(x) = 2(a - 4)x + \lambda \int_0^1 9tf(t)dt$$

Since the integral is independent of x, the solution is a quadratic

$$f(x) = (a - 4)x^2 + bx + c;$$

2) by substituting  $f(x)$  back to the original equation, we get a linear system of equations for b and c:

$$(a - 4)x^2 + bx + c - \lambda \int_0^1 9xtf(t)dt = (a - 4)x^2$$

$$bx + c - \lambda \int_0^1 9xtf(t)dt = 0 \implies \lambda \int_0^1 9xtf(t)dt = bx + c$$

On the left side, there is no constant number so that we can conclude  $c = 0$ ;

$$\text{and } b = \lambda \int_0^1 9tf(t)dt = \lambda \int_0^1 t \cdot 9[(a - 4)t^2 + bt + c]dt$$

$$= 9\lambda \int_0^1 [(a - 4)t^3 + bt^2 + ct] \cdot dt$$

$$= 9\lambda \left[ \frac{(a-4)t^4}{4} + \frac{bt^3}{3} + \frac{ct^2}{2} \Big|_0^1 \right]$$

$$= 9\lambda \left[ \frac{a-4}{4} + \frac{b}{3} + \frac{c}{2} \right] = b$$

$$\therefore b(1 - 3\lambda) - \frac{9}{4}\lambda(2c + a - 4) = 0$$

$$b = \frac{\frac{9}{4}\lambda(2c + a - 4)}{1 - 3\lambda}; c = 0$$

$$\therefore f(x) = (a - 4)x^2 + bx + c = (a - 4)x^2 + \frac{\frac{9}{4}\lambda(2c + a - 4)}{1 - 3\lambda}x + 0$$

$$\therefore f(x) = (a - 4)x \cdot \left(x - \frac{9}{4} \frac{\lambda}{1 - 3\lambda}\right)$$

□



## 9.2 Galerkin Method

### Galerkin Method

Engineering problems in differential equations with boundary conditions generally denote as  $D(U) = 0; B(U) = 0$

To find the function  $U$  which satisfies the given differential equation and boundary conditions, we use:

- 1) Inner Product of Function;
- 2) Basis of a Vector Space

if  $\langle f, g \rangle = \int_a^b f(x)g(x)dx = 0$  then  $f(x)$  and  $g(x)$  are orthogonal

$$f(x) = \sum_{j=0}^{\infty} C_j \phi_j(x)$$

(The Galerkin method is defined with details through an example)

$$\text{Ex: } \frac{d^2 \phi}{dx^2} = x + 1, \quad 0 < x < 1; \quad \phi|_{x=0} = 0, \quad \phi|_{x=1} = 1$$

$$\text{Expand } \phi(x) = C_1 + C_2x + C_3x^2 + C_4x^3$$

$$\text{when } x = 0, \phi(x) = C_1 + C_2 \cdot 0 + C_3 \cdot 0 + C_4 \cdot 0 = C_1 = 0$$

$$C_1 = 0;$$

$$x = 1, \phi(x) = C_1 + C_2 \cdot 1 + C_3 \cdot 1 + C_4 \cdot 1 = 0 + C_2 + C_3 + C_4 = 1$$

$$C_2 = 1 - C_3 - C_4;$$

$$\therefore \tilde{\phi}(x) = 0 + (1 - C_3 - C_4)x + C_3x^2 + C_4x^3$$

$$= x - C_3x - C_4x + C_3x^2 + C_4x^3$$

$$= x + C_3(x^2 - x) + C_4(x^3 - x)$$

$$\implies \frac{d\phi}{dx} = 1 + 2C_3x - C_3 + 3C_4x^2 - C_4;$$

$$\therefore \frac{d^2 \phi}{dx^2} = 2C_3 + 6C_4x$$

$$\text{Inner Product: } \int_0^1 w_i \left( \frac{d^2 \phi}{dx^2} - x - 1 \right) dx = 0$$

$$\therefore \int_0^1 w_i (2C_3 + 6C_4x - x - 1) dx = 0$$

$$\text{let } w_1 = x^2 - x; \quad w_2 = x^3 - x$$

- 1) Plug  $w_1$  back to the integral:

$$\int_0^1 (x^2 - x)(2C_3 + 6C_4x - x - 1) dx = 0$$

$$\int_0^1 (2C_3x^2 + 6C_4x^3 - x^3 - x^2 - 2C_3x - 6C_4x^2 + x^2 + x) dx$$

$$= \int_0^1 (2C_3x^2 + 6C_4x^3 - x^3 - 2C_3x - 6C_4x^2 + x) dx = 0$$

$$\implies \frac{2C_3x^3}{3} + \frac{6C_4x^4}{4} - \frac{x^4}{4} - C_3x^2 - 2C_4x^3 + \frac{x^2}{2} \Big|_0^1 = -\frac{1}{3}C_3 - \frac{1}{2}C_4 + \frac{1}{4} = 0$$

$$\therefore \frac{1}{3}C_3 + \frac{1}{2}C_4 = -\frac{1}{4};$$

2) Plug  $w_2$  back to the integral:

$$\int_0^1 (x^3 - x)(2C_3 + 6C_4x - x - 1)dx = 0$$

$$\int_0^1 (2C_3x^3 + 6C_4x^4 - x^4 - x^3 - 2C_3x - 6C_4x^2 + x^2 + x)dx = 0$$

$$\implies \frac{C_3x^4}{2} + \frac{6C_4x^5}{5} - \frac{x^5}{5} - \frac{x^4}{4} - C_3x^2 - 2C_4x^3 + \frac{x^3}{3} + \frac{x^2}{2} \Big|_0^1 = -\frac{1}{2}C_3 - \frac{4}{5}C_4 + \frac{23}{60} = 0$$

$$\therefore \frac{1}{2}C_3 + \frac{4}{5}C_4 = \frac{23}{60};$$

From (1) and (2), we can get

$$C_3 = \frac{1}{2}, C_4 = \frac{1}{6}, C_2 = 1 - C_3 - C_4 = 1 - \frac{1}{2} - \frac{1}{6} = \frac{1}{3};$$

All in all:

$$C_1 = 0, C_2 = \frac{1}{3}, C_3 = \frac{1}{2}, C_4 = \frac{1}{6}$$

$$\therefore \phi(x) = \frac{1}{3}x + \frac{1}{2}x^2 + \frac{1}{6}x^3 \quad \square$$

### 9.3 The Adomian Decomposition Method

The Adomian Decomposition Method

These methods proved to be reliable and effective for a wide class of equations, differential and integral equations, linear and nonlinear models. The method was applied mostly to ordinary and partial differential equations. The decomposition method can be successfully applied towards linear and nonlinear integral equations.

In the decomposition method we usually express the solution  $u(x)$  of the integral equation in a series form defined as:

$$u(x) = \sum_{n=0}^{\infty} u_n(x) = f(x) + \lambda \int_a^b K(x, t) \left( \sum_{n=0}^{\infty} u_n(t) \right) dt$$

In which means:

$$\begin{aligned} u_0(x) + u_1(x) + u_2(x) + \dots &= f(x) + \lambda \int_a^b K(x, t) u_0(t) dt \\ &+ \lambda \int_a^b K(x, t) u_1(t) dt \\ &+ \lambda \int_a^b K(x, t) u_2(t) dt + \dots \end{aligned}$$

The components  $u_0(x), u_1(x), u_2(x), \dots$  of the unknown function  $u(x)$  are completely determined in a recurrent manner if we set:

$$\begin{aligned} u_0(x) &= f(x), \\ u_1(x) &= \lambda \int_a^b K(x, t) u_0(t) dt, \\ u_2(x) &= \lambda \int_a^b K(x, t) u_1(t) dt, \end{aligned}$$

and so on. The scheme for the determination of the components of the solution  $u(x)$  can be written in a recursive manner as:

$$\begin{aligned} u_0(x) &= f(x), \\ u_{n+1}(x) &= \lambda \int_a^b K(x, t) u_n(t) dt, n \geq 0. \end{aligned}$$

With these components determined, the solution  $u(x)$  is readily determined in a series form using the decomposition. However, for concrete problems, where exact solutions cannot be evaluated, a truncated series  $\sum_{n=0}^k u_n(x)$  is usually used to approximate the solution  $u(x)$  and this can be used for numerical purposes. The following example would illustrate how the decomposition method worked.

Consider the Fredholm integral equation of the second kind

$$u(x) = \frac{9}{10}x^2 + \int_0^1 \frac{1}{2}x^2t^2u(t)dt$$

In this case, it is clear that by using decomposition method,

$$f(x) = \frac{9}{10}x^2, \lambda = 1, K(x, t) = \frac{1}{2}x^2t^2 \text{ so we set:}$$

$$\begin{aligned} u_0(x) &= \frac{9}{10}x^2 \\ u_1(x) &= \frac{9}{10}t^4 dt \end{aligned}$$

$$\begin{aligned}
&= \frac{9}{20}x^2 \int_0^1 t^4 dt = \frac{9}{20}x^2 \cdot \left(\frac{1}{5}t^5 \Big|_0^1\right) \\
&= \frac{9}{100}x^2
\end{aligned}$$

$$\begin{aligned}
u_2(x) &= t^2 \frac{9}{100}t^2 dt \\
&= \frac{9}{200}x^2 \int_0^1 t^4 dt = \frac{9}{200}x^2 \cdot \left(\frac{1}{5}t^5 \Big|_0^1\right) \\
&= \frac{9}{1000}x^2
\end{aligned}$$

and so on, since we note that:

$$u(x) = u_0(x) + u_1(x) + u_2(x) + \dots$$

we can easily obtain the solution in a series form given as:

$$u(x) = \frac{9}{10}x^2 + \frac{9}{100}x^2 + \frac{9}{1000}x^2 + \dots = x^2 \cdot \left(\frac{9}{10} + \frac{9}{100} + \frac{9}{1000} + \dots\right)$$

so that the solution would be:

$$u(x) = x^2 \cdot k, (k \text{ is a constant number})$$

$$\therefore u(x) = x^2 \text{ (in a closed form)}$$

Now consider another Fredholm integral equation of the second kind:

$$u(x) = \sin(x) + \int_{-1}^1 e^{\sin^{-1}(x)} u(t) dt$$

so we set:

$$u_0(x) = \sin(x),$$

$$\begin{aligned}
u_1(x) &= \int_{-1}^1 e^{\sin^{-1}(x)} u_0(t) dt = e^{\sin^{-1}(x)} \int_{-1}^1 \sin(t) dt \\
&= e^{\sin^{-1}(x)} (-\cos(t)) \Big|_{-1}^1 \\
&= (\cos(-1) - \cos(1)) \cdot e^{\sin^{-1}(x)} \\
&= 0 \quad (\cos(-1) - \cos(1) = 0)
\end{aligned}$$

$$u_2(x) = \int_{-1}^1 e^{\sin^{-1}(x)} u_1(t) dt = e^{\sin^{-1}(x)} \cdot (\cos(-1) - \cos(1)) \cdot \int_{-1}^1 e^{\sin^{-1}(t)} dt$$

By using integration by parts:

$$\begin{aligned}
\int_{-1}^1 e^{\sin^{-1}(t)} dt &= t \cdot e^{\sin^{-1}(t)} \Big|_{-1}^1 - \int_{-1}^1 t \cdot e^{\sin^{-1}(t)} \cdot \frac{1}{\sqrt{1-t^2}} dt \\
&= (e^{\sin^{-1}(1)} + e^{\sin^{-1}(-1)}) - \int_{-1}^1 \frac{t \cdot e^{\sin^{-1}(t)}}{\sqrt{1-t^2}} dt \\
&= e^{\frac{\pi}{2}} + e^{-\frac{\pi}{2}} - \int_{-1}^1 \frac{t \cdot e^{\sin^{-1}(t)}}{\sqrt{1-t^2}} dt
\end{aligned}$$

On the other hand, we need u-substitution to solve  $\int_{-1}^1 \frac{t \cdot e^{\sin^{-1}(t)}}{\sqrt{1-t^2}} dt$ , so:

$$\text{let } u = \sin^{-1}(t), du = \frac{1}{\sqrt{1-t^2}} dt$$

$$\therefore t = \sin(u), dt = \sqrt{1-t^2} \cdot du$$

$$\therefore \int \frac{t \cdot e^{\sin^{-1}(t)}}{\sqrt{1-t^2}} dt = \int \sin(u) \cdot e^u du$$

By using another integration by parts:

$$\int \sin(u) \cdot e^u du = \sin(u) \cdot e^u - \int \cos(u) \cdot e^u du$$

$$\int \cos(u) \cdot e^u du = \cos(u) \cdot e^u - \int -\sin(u) \cdot e^u du$$

$$\therefore \int \sin(u) \cdot e^u du = \sin(u) \cdot e^u - \cos(u) \cdot e^u - \int \sin(u) \cdot e^u du$$

$$\therefore 2 \cdot \int \sin(u) \cdot e^u du = e^u \cdot (\sin(u) - \cos(u))$$

$$\text{then } \int \sin(u) \cdot e^u du = \frac{1}{2} e^u (\sin(u) - \cos(u))$$

By converting  $u = \sin^{-1}(t)$  back to the original function, we have:

$$\begin{aligned} \int_{-1}^1 \frac{t \cdot e^{\sin^{-1}(t)}}{\sqrt{1-t^2}} dt &= \frac{1}{2} e^{\sin^{-1}(t)} (\sin(\sin^{-1}(t)) - \cos(\sin^{-1}(t))) \Big|_{-1}^1 \\ &= \frac{1}{2} e^{\sin^{-1}(t)} (t - \cos(\sin^{-1}(t))) \Big|_{-1}^1 \\ &= \frac{1}{2} e^{\sin^{-1}(1)} (1 - \cos(\sin^{-1}(1))) - \frac{1}{2} e^{\sin^{-1}(-1)} (-1 - \cos(\sin^{-1}(-1))) \\ &= \frac{1}{2} e^{\frac{\pi}{2}} \cdot (1 - 0) - \frac{1}{2} e^{-\frac{\pi}{2}} \cdot (-1 - 0) \\ &= \frac{1}{2} e^{\frac{\pi}{2}} + \frac{1}{2} e^{-\frac{\pi}{2}} \end{aligned}$$

$$\begin{aligned} \therefore \int_{-1}^1 e^{\sin^{-1}(t)} dt &= e^{\frac{\pi}{2}} + e^{-\frac{\pi}{2}} - (12e\pi 2 + 12e - \pi 2) \\ &= 12e\pi 2 + 12e - \pi 2 \end{aligned}$$

$$\begin{aligned} \text{so } u_2(x) &= e^{\sin^{-1}(x)} \cdot (\cos(-1) - \cos(1)) \cdot (12e\pi 2 + 12e - \pi 2) \\ &= 0 \quad (\cos(-1) - \cos(1) = 0) \end{aligned}$$

$$\begin{aligned} \therefore u(x) &= u_0(x) + u_1(x) + u_2(x) + \dots \\ &= \sin(x) + 0 + 0 + \dots = \sin(x) \end{aligned}$$

All in all,  $u(x) = \sin(x)$  in closed form.

□

## 9.4 The Modified Decomposition Method

### The Modified Decomposition Method

For cases where the non-homogeneous part consists of a combination of many terms, the modified decomposition method is recommended.

This modified technique will be carried out with promising results in Volterra integral evaluations, avoiding the cumbersome integrations of other methods.

In the modified method, the given function  $f(x)$  would be split into two parts defined as:

$$f(x) = f_0(x) + f_1(x),$$

where  $f_0(x)$  consists of number of terms of  $f(x)$ , and  $f_1(x)$  includes the remaining terms of  $f(x)$ .

With new defined  $f(x)$ , the supposed integral equation would be:

$$u(x) = f_0(x) + f_1(x) + \lambda \int_a^b K(x, t)u(t)dt, \quad a \leq x \leq b.$$

$$\begin{aligned} u(x) &= u_0(x) + u_1(x) + u_2(x) + \dots u_n(x) \\ &= f_0(x) + f_1(x) + \lambda \int_a^b K(x, t)u_0(t)dt + \lambda \int_a^b K(x, t)u_1(t)dt + \lambda \int_a^b K(x, t)u_2(t)dt + \\ &\dots + \lambda \int_a^b K(x, t)u_n(t)dt \end{aligned}$$

The components  $u_0(x), u_1(x), u_2(x) \dots$  of the unknown function  $u(x)$  can be completely determined in a recurrent manner if  $f_0(x)$  is assigned only to the zeroth component  $u_0(x)$ , whereas the function  $f_1(x)$  will be added to the formula of the first component  $u_1(x)$  given before, which means if we set:

$$u_0(x) = f_0(x),$$

$$u_1(x) = f_1(x) + \lambda \int_a^b K(x, t)u_0(t)dt,$$

$$u_2(x) = \lambda \int_a^b K(x, t)u_1(t)dt,$$

$$u_3(x) = \lambda \int_a^b K(x, t)u_2(t)dt, \text{ and so on...}$$

$$\text{Then } u_{n+1}(x) = \lambda \int_a^b K(x, t)u_n(t)dt, \quad n \geq 1.$$

The modified decomposition scheme can be explained by an illustrative example, consider a Fredholm integral equation:

$$u(x) = e^{3x} - \frac{1}{9}(2e^3 + 1)x + \int_0^1 xtu(t)dt$$

so the function  $f(x)$  can be split into:

$$f_0(x) = e^{3x},$$

$$f_1(x) = -\frac{1}{9}(2e^3 + 1)x$$

Therefore we set:

$$u_0(x) = f_0(x) = e^{3x},$$

$$\begin{aligned}
u_1(x) &= -\frac{1}{9}(2e^3 + 1)x + \int_0^1 xt u_0(t) dt = -\frac{1}{9}(2e^3 + 1)x + x \int_0^1 t e^{3t} dt \\
\int_0^1 t e^{3t} dt &= t \cdot \frac{1}{3} e^{3t} \Big|_0^1 - \frac{1}{3} \int_0^1 e^{3t} dt \\
&= \left(\frac{1}{3} e^3 - 0\right) - \left(\frac{1}{9} e^{3t} \Big|_0^1\right) = \frac{1}{3} e^3 - \left(\frac{1}{9} e^3 - \frac{1}{9}\right) = \frac{1}{3} e^3 - \frac{1}{9} e^3 + \frac{1}{9} \\
\therefore u_1(x) &= -\frac{1}{9}(2e^3 + 1)x + \left(\frac{1}{3} e^3 - \frac{1}{9} e^3 + \frac{1}{9}\right)x \\
&= x \left(-\frac{2}{9} e^3 - \frac{1}{9} + \frac{1}{3} e^3 - \frac{1}{9} e^3 + \frac{1}{9}\right) \\
&= 0
\end{aligned}$$

Since  $u_1(x) = 0$ , we can conclude that  $u_n(x) = 0$ , for  $n \geq 1$ . Then the exact solution of the original function would be:

$$\begin{aligned}
u(x) &= u_0(x) + u_1(x) + \dots = u_0(x) + 0 = u_0(x) \\
\therefore u(x) &= e^{3x}
\end{aligned}$$

Another Example: consider a Fredholm integral equation:

$$u(x) = x \tan^{-1}(x) + \left(\frac{\pi}{4} - \frac{1}{2}\right)x - \int_0^1 x u(t) dt$$

so the function  $f(x)$  can be split into:

$$f_0(x) = x \tan^{-1}(x);$$

$$f_1(x) = \left(\frac{\pi}{4} - \frac{1}{2}\right)x$$

Therefore we set:

$$u_0(x) = f_0(x) = x \tan^{-1}(x),$$

$$u_1(x) = \left(\frac{\pi}{4} - \frac{1}{2}\right)x - \int_0^1 x u_0(t) dt = \left(\frac{\pi}{4} - \frac{1}{2}\right)x - x \int_0^1 t \cdot \tan^{-1}(t) dt,$$

$$\begin{aligned}
\int_0^1 t \cdot \tan^{-1}(t) dt &= \frac{1}{2} t^2 \cdot \tan^{-1}(t) \Big|_0^1 - \int_0^1 \frac{1}{2} t^2 \cdot \frac{1}{1+t^2} dt \\
&= \left(\frac{1}{2} \tan^{-1}(1) - 0\right) - \frac{1}{2} \int_0^1 \frac{t^2}{1+t^2} dt \\
&= \frac{1}{2} \cdot \frac{\pi}{4} - \frac{1}{2} \int_0^1 \frac{1+t^2}{1+t^2} - \frac{1}{1+t^2} dt \\
&= \frac{\pi}{8} - \frac{1}{2} \int_0^1 1 - \frac{1}{1+t^2} dt \\
&= \frac{\pi}{8} - \frac{1}{2} \cdot \left[(t - \tan^{-1}(t)) \Big|_0^1\right] \\
&= \frac{\pi}{8} - \frac{1}{2} \left[1 - \frac{\pi}{4}\right] \\
&= \frac{\pi}{4} - \frac{1}{2}
\end{aligned}$$

$$\therefore u_1(x) = \left(\frac{\pi}{4} - \frac{1}{2}\right)x - x \cdot \left(\frac{\pi}{4} - \frac{1}{2}\right) = 0$$

Since  $u_1(x) = 0$ , we can conclude that  $u_n(x) = 0$ , for  $n \geq 1$ . Then the exact solution of the original function would be:

$$u(x) = u_0(x) + u_1(x) + \dots = u_0(x) + 0 = u_0(x)$$

$$\therefore u(x) = x \tan^{-1}(x) \quad \square$$

## 9.5 The Volume and Surface Area of the Spherical Pyramid

### The Volume and Surface Area of the Spherical Pyramid

When the Cartesian Coordinates are transferred in the spherical coordinate system:

$$x = r \sin \theta \cos \varphi$$

$$y = r \sin \theta \sin \varphi$$

$$z = r \cos \theta$$

where  $r$  is the radius,  $\theta$  is the polar angle from the positive  $z$ -axis with  $0 \leq \theta \leq \pi$ , and  $\varphi$  is the azimuthal angle in the  $x$ - $y$  plane from the  $x$ -axis with  $0 \leq \varphi \leq 2\pi$ .

In order to find the volume of a shape in the spherical coordinate system, the triple integral is going to be used based on

$$dV = r^2 \sin \theta dr d\varphi d\theta$$

and the surface area of a shape is calculated through a double intergral based on

$$dA = r^2 \sin \theta d\varphi d\theta$$

In order to calculate the volume and the surface are of the Spherical Pyramid, here are the equations of the shape:

$$x = 1.43 \cdot \cos(0.5\theta) \sin(\theta) \cos(\varphi)$$

$$y = 1.43 \cdot \sin(0.5\theta) \sin(\theta) \sin(\varphi)$$

$$z = \cos(\theta)$$

For my own shape, the radius of the Spherical Pyramid is assumed to be  $0 \leq r \leq 1$ . The polar angle is  $0 \leq \theta \leq \pi$ , and the azimuthal angle is  $0 \leq \varphi \leq 2\pi$ .

Therefore, the volume of the Spherical Pyramid would be a triple integral as:

$$\int_0^\pi \int_0^{2\pi} \int_0^1 r^2 \sin \theta dr d\varphi d\theta$$

$$\text{where } r^2 = x^2 + y^2 + z^2$$

$$= 1.43^2 \cdot \cos^2(0.5\theta) \sin^2(\theta) \cos^2(\varphi) + 1.43^2 \cdot \sin^2(0.5\theta) \sin^2(\theta) \sin^2(\varphi) + \cos^2(\theta)$$

$$= 1.43^2 \sin^2(\theta) [\cos^2(0.5\theta) \cos^2(\varphi) + \sin^2(0.5\theta) \sin^2(\varphi)] + \cos^2(\theta)$$

By using trigonometric identities,

$$\cos^2(0.5\theta) = \frac{1+\cos(\theta)}{2}; \quad \sin^2(0.5\theta) = \frac{1-\cos(\theta)}{2},$$

$$\text{therefore, } \cos^2(0.5\theta) \cos^2(\varphi) + \sin^2(0.5\theta) \sin^2(\varphi)$$

$$= \frac{1+\cos(\theta)}{2} \cdot \cos^2(\varphi) + \frac{1-\cos(\theta)}{2} \cdot \sin^2(\varphi)$$

$$= \frac{1}{2}(\cos^2(\theta) + \sin^2(\theta)) + \frac{\cos(\theta)}{2} \cdot (\cos^2(\varphi) - \sin^2(\varphi))$$



According to trigonometric identities,

$$\cos^2(\theta) + \sin^2(\theta) = 1 \text{ and } \cos^2(\varphi) - \sin^2(\varphi) = \cos(2\varphi)$$

$$\begin{aligned} \text{therefore, } \cos^2(0.5\theta) \cos^2(\varphi) + \sin^2(0.5\theta) \sin^2(\varphi) &= \frac{1}{2} + \frac{\cos(\theta)}{2} \cdot \cos(2\varphi) \\ &= \frac{1}{2} \cdot (1 + \cos(\theta) \cos(2\varphi)) \end{aligned}$$

$$\text{then } r^2 = 1.43^2 \sin^2(\theta) \cdot \frac{1}{2}(1 + \cos(\theta) \cos(2\varphi)) + \cos^2(\theta)$$

The new triple integral would become:

$$\begin{aligned} &\int_0^\pi \int_0^{2\pi} \int_0^1 [1.43^2 \sin^2(\theta) \frac{1}{2}(1 + \cos(\theta) \cos(2\varphi)) + \cos^2(\theta)] \cdot \sin(\theta) dr d\varphi d\theta \\ &= \int_0^\pi \int_0^{2\pi} \int_0^1 [\frac{1.43^2}{2} \sin^3(\theta) + \frac{1.43^2}{2} \sin^3(\theta) \cos(\theta) \cos(2\varphi) + \sin(\theta) \cos^2(\theta)] dr d\varphi d\theta \end{aligned}$$

The integral can be solved separately part by part.

$$\begin{aligned} \text{First part: } &\int_0^\pi \int_0^{2\pi} \int_0^1 \frac{1.43^2}{2} \sin^3(\theta) dr d\varphi d\theta = \int_0^\pi \int_0^{2\pi} \frac{1.43^2}{2} \sin^3(\theta) \cdot r|_0^1 d\varphi d\theta \\ &= \int_0^{2\pi} \int_0^\pi \frac{1.43^2}{2} \sin^3(\theta) d\theta d\varphi = \int_0^{2\pi} \int_0^\pi \frac{1.43^2}{2} (1 - \cos^2(\theta)) \sin(\theta) d\theta d\varphi \end{aligned}$$

By using u-substitution: let  $u = \cos(\theta)$ , then  $du = -\sin(\theta)d\theta$ , we have

$$\begin{aligned} &\int_0^\pi \frac{1.43^2}{2} (1 - u^2) \cdot -du = \frac{1.43^2}{2} \int_0^\pi (u^2 - 1) du = \frac{1.43^2}{2} \cdot [\frac{1}{3}u^3 - u] \\ &= \frac{1.43^2}{2} \cdot [\frac{1}{3} \cos^3(\theta) - \cos(\theta)]_0^\pi = \frac{1.43^2}{2} \cdot [(-\frac{1}{3} + 1) - (\frac{1}{3} - 1)] \\ &= \frac{1.43^2}{2} \cdot \frac{4}{3} = \frac{2 \cdot 1.43^2}{3} \end{aligned}$$

and then the integral for the first part becomes:

$$\int_0^{2\pi} \frac{2 \cdot 1.43^2}{3} d\varphi = \frac{2 \cdot 1.43^2}{3} \varphi|_0^{2\pi} = \frac{4 \cdot 1.43^2}{3} \pi$$

$$\text{Second part: } \int_0^\pi \int_0^{2\pi} \int_0^1 \frac{1.43^2}{2} \sin^3(\theta) \cos(\theta) \cos(2\varphi) dr d\varphi d\theta$$

$$\begin{aligned} &= \int_0^\pi \int_0^{2\pi} \frac{1.43^2}{2} \sin^3(\theta) \cos(\theta) \cos(2\varphi) r|_0^1 d\varphi d\theta = \int_0^\pi \int_0^{2\pi} \frac{1.43^2}{2} \sin^3(\theta) \cos(\theta) \cos(2\varphi) d\varphi d\theta \\ &= \int_0^\pi \frac{1.43^2}{2} \sin^3(\theta) \cos(\theta) \cdot \frac{1}{2} \sin(2\varphi)|_0^{2\pi} d\theta = \frac{1.43^2}{4} \int_0^\pi \sin^3(\theta) \cos(\theta) \cdot [\sin(4\pi) - \\ &\sin(0)] d\theta \\ &= \frac{1.43^2}{4} \int_0^\pi \sin^3(\theta) \cos(\theta) \cdot 0 d\theta = 0 \end{aligned}$$

$$\text{Third part: } \int_0^\pi \int_0^{2\pi} \int_0^1 \sin(\theta) \cos^2(\theta) dr d\varphi d\theta$$

$$\begin{aligned}
&= \int_0^\pi \int_0^{2\pi} \sin(\theta) \cos^2(\theta) r \Big|_0^1 d\varphi d\theta = \int_0^\pi \int_0^{2\pi} \sin(\theta) \cos^2(\theta) d\varphi d\theta \\
&= \int_0^\pi \sin(\theta) \cos^2(\theta) \varphi \Big|_0^{2\pi} d\theta = 2\pi \cdot \int_0^\pi \sin(\theta) \cos^2(\theta) d\theta
\end{aligned}$$

By using u-substitution: let  $u = \cos(\theta)$ , then  $du = -\sin(\theta)d\theta$ , we have

$$\begin{aligned}
&-2\pi \cdot \int_0^\pi u^2 du = -2\pi \cdot \left[ \frac{1}{3} u^3 \Big|_0^\pi \right] = -2\pi \cdot \left[ \frac{1}{3} \cos^3(\theta) \Big|_0^\pi \right] \\
&= -2\pi \cdot \left[ \frac{1}{3} \cos^3(\pi) - \frac{1}{3} \cos(0) \right] = -2\pi \cdot \left[ -\frac{2}{3} \right] = \frac{4}{3}\pi
\end{aligned}$$

Overall, the final integral is equal to the sum of three separated parts:

$$\begin{aligned}
&\int_0^\pi \int_0^{2\pi} \int_0^1 [1.43^2 \sin^2(\theta) \frac{1}{2}(1 + \cos(\theta) \cos(2\varphi)) + \cos^2(\theta)] \cdot \sin(\theta) dr d\varphi d\theta \\
&= \frac{4 \cdot 1.43^2}{3} \pi + 0 + \frac{4}{3} \pi = \frac{4 \cdot 1.43^2 + 4}{3} \pi = 4.06\pi
\end{aligned}$$

The surface area of the shape would be a double integral as:

$$\begin{aligned}
&\int_0^\pi \int_0^{2\pi} r^2 \sin \theta d\varphi d\theta = r^2 \int_0^\pi \sin(\theta) \cdot \varphi \Big|_0^{2\pi} d\theta \\
&= 2\pi r^2 \int_0^\pi \sin(\theta) d\theta = 2\pi r^2 \cdot (-\cos(\theta) \Big|_0^\pi) = 2\pi r^2 \cdot 2 = 4\pi r^2
\end{aligned}$$

since  $r^2 = 1.43^2 \cdot \cos^2(0.5\theta) \sin^2(\theta) \cos^2(\varphi) + 1.43^2 \cdot \sin^2(0.5\theta) \sin^2(\theta) \sin^2(\varphi) + \cos^2(\theta)$ , then the boundary of the radius would be the sum of three separated parts as:

$$\begin{aligned}
0 &\leq |1.432 \cdot \cos 2(0.5\theta) \sin 2(\theta) \cos 2(\varphi)| \leq 1.43^2 \\
0 &\leq |1.43^2 \cdot \sin^2(0.5\theta) \sin^2(\theta) \sin^2(\varphi)| \leq 1.43^2 \\
0 &\leq |\cos^2(\theta)| \leq 1
\end{aligned}$$

therefore, we have:  $0 \leq r^2 \leq (2 \cdot 1.43^2 + 1)$ . So the surface area of the Spherical Pyramid is bounded as:

$$0 \leq 4\pi r^2 \leq 4 \cdot \pi \cdot (2 \cdot 1.43^2 + 1) \implies 0 \leq 4\pi r^2 \leq 20.3592\pi$$

Therefore, the volume of the Spherical Pyramid is about  $4.06\pi$  units cube, and the surface area is bounded under  $20.3592\pi$  units square. The Spherical Pyramid is proved to be closed and bounded, which is applicable to use the Green Theorem.

## 9.6 The Weakly-Singular Fredholm Integral Equations

The Weakly-Singular Fredholm Integral Equations

The weakly-singular Fredholm integral equations of the second kind is formed as:

$$u(x) = f(x) + \int_0^1 \frac{1}{\sqrt{x-t}} u(t) dt, \quad x \in [0, 1],$$

and can also be generalized as:

$$u(x) = f(x) + \int_0^1 \frac{1}{(x-t)^\alpha} u(t) dt, \quad 0 < \alpha < 1, \quad x \in [0, 1],$$

where  $u(t)$  is the unknown solution. The main goal of solving weakly-singular Fredholm integral equations was the determination of numerical approximations of the solutions. The modified decomposition method and the noise term phenomenon to determine exact solutions of such singular integral equations.

The modified decomposition method decomposes the function  $f(x)$  into two components as  $f_0(x)$  and  $f_1(x)$ , and the computation is minimized by using the modified decomposition method. The modified recurrence relation is given as:

$$\begin{aligned} u_0(x) &= f_0(x), \\ u_1(x) &= f_1(x) + \int_a^b K(x, t) u_0(t) dt, \\ u_{n+1}(x) &= \int_a^b K(x, t) u_n(t) dt, \quad n \geq 1. \end{aligned}$$

The noise terms are defined as the identical terms with opposite signs that may appear within the components  $u_n(x)$ , for  $n \geq 0$ . The noise terms will provide the exact solution by using only the first two iterations, if it appears especially within both of the components  $u_0(x)$  and  $u_1(x)$ . By canceling the noise terms for  $u_0(x)$ , the remaining non-canceled terms of  $u_0(x)$  may give the exact solution, which can be verified through substitution into the original equation. The modified decomposition method and the noise terms phenomenon would be applied when it is appropriate.

Example 1: Consider the weakly-singular Fredholm integral equation

$$u(x) = 3 + 6\sqrt{x-1} - 6\sqrt{x} + \int_0^1 \frac{u(t)}{\sqrt{x-t}} dt, \quad 0 \leq x \leq 1.$$

We first decompose  $f(x)$  into two parts defined as:

$$\begin{aligned} f_0(x) &= 3, \\ f_1(x) &= 6\sqrt{x-1} - 6\sqrt{x}. \end{aligned}$$

The modified decomposition method admits the use of the modified recurrence relation as:

$$\begin{aligned} u_0(x) &= 3, \\ u_1(x) &= 6\sqrt{x-1} - 6\sqrt{x} + \int_0^1 \frac{u_0(t)}{\sqrt{x-t}} dt = 6\sqrt{x-1} - 6\sqrt{x} + \int_0^1 \frac{3}{\sqrt{x-t}} dt \\ &= 6\sqrt{x-1} - 6\sqrt{x} + 3 \int_0^1 \frac{1}{\sqrt{x-t}} dt \end{aligned}$$

$$\begin{aligned}
&= 6\sqrt{x-1} - 6\sqrt{x} + 3(-2\sqrt{x-t}|_0^1) \\
&= 6\sqrt{x-1} - 6\sqrt{x} + 3(-2\sqrt{x-1} + 2\sqrt{x}) \\
&= 6\sqrt{x-1} - 6\sqrt{x} - 6\sqrt{x-1} + 6\sqrt{x} \\
&= 0
\end{aligned}$$

This gives the exact solution as:  $u(x) = 0$ .

Example 2: Consider the weakly-singular Fredholm integral equation

$$u(x) = 10x - 9x^{\frac{5}{3}} + 6(x-1)^{\frac{2}{3}} + 9x(x-1)^{\frac{2}{3}} + \int_0^1 \frac{u(t)}{(x-t)^{\frac{1}{3}}} dt.$$

First of all,  $f(x)$  should be decomposed into two parts defined as:

$$f_0(x) = 10x,$$

$$f_1(x) = -9x^{\frac{5}{3}} + 6(x-1)^{\frac{2}{3}} + 9x(x-1)^{\frac{2}{3}}.$$

The modified decomposition method admits the use of the modified recurrence defined as:

$$u_0(x) = 10x,$$

$$\begin{aligned}
u_1(x) &= -9x^{\frac{5}{3}} + 6(x-1)^{\frac{2}{3}} + 9x(x-1)^{\frac{2}{3}} + \int_0^1 \frac{u_0(t)}{(x-t)^{\frac{1}{3}}} dt \\
&= -9x^{\frac{5}{3}} + 6(x-1)^{\frac{2}{3}} + 9x(x-1)^{\frac{2}{3}} + \int_0^1 \frac{10t}{(x-t)^{\frac{1}{3}}} dt \\
&= -9x^{\frac{5}{3}} + 6(x-1)^{\frac{2}{3}} + 9x(x-1)^{\frac{2}{3}} + 10 \cdot \int_0^1 \frac{t}{(x-t)^{\frac{1}{3}}} dt
\end{aligned}$$

In order to solve  $\int_0^1 \frac{t}{(x-t)^{\frac{1}{3}}} dt$ , we need to use the integration by parts:

$$\begin{aligned}
\int_0^1 \frac{t}{(x-t)^{\frac{1}{3}}} dt &= \int_0^1 t \cdot (x-t)^{-\frac{1}{3}} dt \\
&= -\frac{3}{2}(x-t)^{\frac{2}{3}} \cdot t \Big|_0^1 - \int_0^1 -\frac{3}{2}(x-t)^{\frac{2}{3}} \cdot 1 dt \\
&= -\frac{3}{2}(x-1)^{\frac{2}{3}} + \frac{3}{2} \cdot \int_0^1 (x-t)^{\frac{2}{3}} dt \\
&= -\frac{3}{2}(x-1)^{\frac{2}{3}} + \frac{3}{2} \cdot \left(-\frac{3}{5}(x-t)^{\frac{5}{3}} \Big|_0^1\right) \\
&= -\frac{3}{2}(x-1)^{\frac{2}{3}} - \frac{9}{10}(x-1)^{\frac{5}{3}} + \frac{9}{10}x^{\frac{5}{3}}
\end{aligned}$$

$$\begin{aligned}
\therefore u_1(x) &= -9x^{\frac{5}{3}} + 6(x-1)^{\frac{2}{3}} + 9x(x-1)^{\frac{2}{3}} \\
&\quad + 10 \cdot \left(-\frac{3}{2}(x-1)^{\frac{2}{3}} - \frac{9}{10}(x-1)^{\frac{5}{3}} + \frac{9}{10}x^{\frac{5}{3}}\right) = 0
\end{aligned}$$

so the noise terms would be cancelled, therefore the exact solution would be given as:

$$u(x) = 10x.$$

□

## 9.7 The Weakly-Singular Fredholm Integral Equations (Nonlinear)

### Nonlinear Weakly-Singular Fredholm Integral Equations

The nonlinear weakly-singularly Fredholm integral equations are of the form

$$u(x) = f(x) + \int_0^1 \frac{1}{\sqrt{|x-t|}} F(u(t)) dt, \quad x \in [0, 1]$$

and its generalized form is given by

$$u(x) = f(x) + \int_0^1 \frac{1}{|g(x)-g(t)|^\alpha} F(u(t)) dt, \quad 0 < \alpha < 1, \quad x \in [0, 1]$$

where  $F(u(t))$  is a nonlinear function of  $u(t)$ , such as  $u^2(x)$ ,  $u^3(x)$ ,  $e^{u(x)}$  etc.

The nonlinear weakly-singular Fredholm integral equations often arise in practical applications such as Dirichlet problems. The function  $f(x)$  is a given real-valued function. The kernel is called weakly-singular because singularity can be removed by an appropriate transformation. The modified Adomian decomposition method and the noise terms phenomenon would be used to determine the exact solutions for nonlinear weakly-singular Fredholm integral equations.

By using the Adomian decomposition method, the solution of any equations would be decomposed as an infinite series of componenets, where these componenets are determined by a recurrence relation. So the modified method proposes the modified recurrence relation given as:

$$\begin{aligned} u_0(x) &= f_0(x), \\ u_1(x) &= f_1(x) + \int_a^b K(x, t) A_0(t) dt, \\ u_{n+1}(x) &= \int_a^b K(x, t) A_n(t) dt, \quad n \geq 1 \end{aligned}$$

Using the modified decomposition method would not only minimize the computations but also avoid the use of the higher order Adomian polynomials. The convergence of the solution can be faciliated by using the noise terms phenomenon. Because the noise terms are defined as the identical terms with opposite signs, the size of the calculations will be minimized, which validates the efficiency and reliability of the modified method and the noise terms phenomenon. The following examples would illusrtae more clearly the use of the modified decomposition method and the noise terms phenomenon.

Example 1: Consider the nonlinear weakly-singular Fredholm integral equation

$$u(x) = x - \frac{2}{3(x\sqrt{x} + \sqrt{|x^3-1|})} + \int_0^1 \frac{u^2(t)}{\sqrt{|x^3-t^3|}} dt, \quad 0 \leq x \leq 1$$

By using the modified decomposition method, the data function  $f(x)$  would be decomposed into two parts as

$$\begin{aligned} f_0(x) &= x, \\ f_1(x) &= -\frac{2}{3(x\sqrt{x} + \sqrt{|x^3-1|})} \end{aligned}$$

Consequently, we set the modified recurrence relation as

$$u_0(x) = x,$$

$u_1(x) = -\frac{2}{3(x\sqrt{x} + \sqrt{|x^3-1|})} + \int_0^1 \frac{A_0(t)}{\sqrt{|x^3-t^3|}} dt$ , where the zeroth-order Adomian polynomial  $A_0(x) = u_0^2(x)$ , so

$$\begin{aligned} u_1(x) &= -\frac{2}{3(x\sqrt{x} + \sqrt{|x^3-1|})} + \int_0^1 \frac{t^2}{\sqrt{|x^3-t^3|}} dt \\ &= -\frac{2}{3(x\sqrt{x} + \sqrt{|x^3-1|})} + \left(-\frac{2}{3} \cdot |x^3 - t^3|^{\frac{1}{2}} \Big|_0^1\right) \\ &= -\frac{2}{3(x\sqrt{x} + \sqrt{|x^3-1|})} + \left(-\frac{2}{3}\sqrt{|x^3-1|} + \frac{2}{3}\sqrt{|x^3|}\right) \\ &= -\frac{2}{3(x^{\frac{3}{2}} + (|x^3-1|)^{\frac{1}{2}})} + \frac{2}{3}x^{\frac{3}{2}} - \frac{2}{3}(|x^3-1|)^{\frac{1}{2}} \\ &= -\frac{2}{3} \cdot \frac{1}{x^{\frac{3}{2}} + (|x^3-1|)^{\frac{1}{2}}} + \frac{2x^{\frac{3}{2}}}{3} - \frac{2(|x^3-1|)^{\frac{1}{2}}}{3} \\ &= -\frac{2}{3} \cdot \frac{1}{x^{\frac{3}{2}} + (|x^3-1|)^{\frac{1}{2}}} \cdot \frac{x^{\frac{3}{2}} - (|x^3-1|)^{\frac{1}{2}}}{x^{\frac{3}{2}} - (|x^3-1|)^{\frac{1}{2}}} + \frac{2x^{\frac{3}{2}} - 2(|x^3-1|)^{\frac{1}{2}}}{3} \\ &= -\frac{2}{3} \cdot \frac{x^{\frac{3}{2}} - (|x^3-1|)^{\frac{1}{2}}}{x^3 - (x^3-1)} + \frac{2x^{\frac{3}{2}} - 2(|x^3-1|)^{\frac{1}{2}}}{3} \\ &= -\frac{2}{3} \cdot \frac{x^{\frac{3}{2}} - (|x^3-1|)^{\frac{1}{2}}}{x^3 - x^3 + 1} + \frac{2}{3} \cdot (x^{\frac{3}{2}} - (|x^3-1|)^{\frac{1}{2}}) \\ &= -\frac{2}{3} \cdot (x^{\frac{3}{2}} - (|x^3-1|)^{\frac{1}{2}}) + \frac{2}{3} \cdot (x^{\frac{3}{2}} - (|x^3-1|)^{\frac{1}{2}}) = 0 \end{aligned}$$

Since  $u_1(x) = 0$ , it can be concluded that the other components  $u_r(x) = 0$  for  $r \geq 1$  would vanish in the limit. Therefore the exact solution would be:

$$u(x) = x \quad \square$$